

Relating Graph Neural Networks to Structural Causal Models

Matej Zečević¹, Devendra Singh Dhami¹, Petar Veličković², Kristian Kersting¹

¹Computer Science Department, TU Darmstadt, ²DeepMind

Abstract

Causality can be described in terms of a structural causal model (SCM) that carries information on the variables of interest and their mechanistic relations. For most processes of interest the underlying SCM will only be partially observable, thus causal inference tries to leverage any exposed information. Graph neural networks (GNN) as universal approximators on structured input pose a viable candidate for causal learning, suggesting a tighter integration with SCM. To this effect we present a theoretical analysis from first principles that establishes a novel connection between GNN and SCM while providing an extended view on general neural-causal models. We then establish a new model class for GNN-based causal inference that is necessary and sufficient for causal effect identification. Our empirical illustration on simulations and standard benchmarks validate our theoretical proofs.

Introduction

Understanding causal interactions is central to human cognition and thereby of high value to science, engineering, business, and law (Penn and Povinelli 2007). Developmental psychology has shown how children explore similar to the manner of scientist, all by asking "What if?" and "Why?" type of questions (Gopnik 2012; Buchsbaum et al. 2012; Pearl and Mackenzie 2018), while artificial intelligence research dreams of automating the scientist's manner (McCarthy 1998; McCarthy and Hayes 1981; Steinruecken et al. 2019). Deep learning has brought optimizable universality in approximation which refers to the fact that for any function there will exist a neural network that is close in approximation to arbitrary precision (Cybenko 1989; Hornik 1991). This capability has been corroborated by tremendous success in various applications (Krizhevsky, Sutskever, and Hinton 2012; Mnih et al. 2013; Vaswani et al. 2017). Thereby, combining causality with deep learning is of critical importance for research on the verge to a human-level intelligence. Preliminary attempts on a tight integration for so-called neural-causal models (Xia et al. 2021; Pawłowski, Castro, and Glocker 2020) exist and show to be promising towards the dream of a system that performs causal inferences at the same scale of effectiveness as modern-day neural modules in their most impressive applications. While causality has been thoroughly formalized within the last decade (Pearl 2009; Peters, Janzing, and Schölkopf 2017),

deep learning on the other hand saw its success in practical applications with theoretical breakthroughs remaining in the few. Bronstein et al. (2017) pioneer the notion of geometric deep learning and an important class of neural networks that follows from the geometric viewpoint and generalize to modern architectures is the graph neural network (GNN) (Veličković et al. 2017; Kipf and Welling 2016a; Gilmer et al. 2017). Similar to other specialized neural networks, the GNN has resulted in state-of-the-art performance in specialized applications like drug discovery (Stokes et al. 2020) and more recently on ETA prediction in google maps (Derrow-Pinion et al. 2021). These specialities, to which we refer to as inductive biases, can leverage otherwise provably impossible inferences (Gondal et al. 2019). As the name suggests, the GNN places an inductive bias on the structure of the input i.e., the input's dimensions are related such that they form a graph structure. To link back to causality, at its core lies a Structural Causal Model (SCM) which is considered to be the model of reality responsible for data-generation. The SCM implies a graph structure over its modelled variables, and since GNN work on graphs, a closer inspection on the relation between the two models seems reasonable towards progressing research in neural-causal AI. Instead of taking inspiration from causality's principles for improving machine learning (Mitrovic et al. 2020), we instead show how GNN can be used to perform causal computations i.e., how causality can emerge within neural models. To be more precise on the term causal inference: we refer to the modelling of Pearl's Causal Hierarchy (PCH) (Bareinboim et al. 2020). That is, we are given partial knowledge on the SCM in the form of e.g. the (partial) causal graph and/or data from the different levels of the hierarchy. Overall, we make a number of key contributions: (1) We derive from first principles a theoretical connection between GNN and SCM; (2) We define a more fine-grained NCM; (3) We formalize interventions for GNN and by this establish a new neural-causal model class that makes use of auto-encoders; (4) We provide theoretical results and proofs on the feasibility, expressivity, and identifiability of this new model class while relating to existing work (5) We empirically examine our theoretical model for practical causal inference on identification and estimation tasks. We make our code repository publicly available at: <https://anonymous.4open.science/r/Relating-Graph-Neural-Networks-to-Structural-Causal-Models-A8EE>.

Background and Related Work

Let us briefly review the background on variational methods for generative modelling, on graph neural networks as non-parametric function approximator that leverage structural information, and conclusively on causal inference through the process of intervention/mutilation.

Notation. We denote indices by lower-case letters, functions by the general form $g(\cdot)$, scalars or random variables interchangeably by upper-case letters, vectors, matrices and tensors with different boldface font $\mathbf{v}, \mathbf{V}, \mathbf{V}$ respectively, and probabilities of a set of random variables \mathbf{X} as $p(\mathbf{X})$.

Variational Inference. Similar to the notions of disentanglement and causality, latent variable models propose the existence of a-priori unknown variables \mathbf{Z} to jointly model the phenomenon of interest with observed data, $p(\mathbf{X}, \mathbf{Z})$. The Variational Inference (VI) machine learning technique makes use of optimization, as an alternative to Markov chain Monte Carlo sampling (MCMC) approaches, for overcoming the curse of dimensionality¹ when estimating probability distributions (Jordan et al. 1999; Blei, Kucukelbir, and McAuliffe 2017). In this Bayesian setting, the inference problem amounts to estimating the latent variable conditional $p(\mathbf{Z} \mid \mathbf{X})$ through the closest density of a pre-specified family \mathcal{Q} , that is,

$$q^*(\mathbf{Z}) = \arg \min_{q \in \mathcal{Q}} \text{KL}(q(\mathbf{Z}) \parallel p(\mathbf{Z} \mid \mathbf{X})) \quad (1)$$

where the distance measure is set to be the Kullback-Leibler divergence. Inspecting Bayes Rule exposes that $p(\mathbf{Z} \mid \mathbf{X}) = \frac{p(\mathbf{X}, \mathbf{Z})}{p(\mathbf{X})}$ where the evidence in the denominator is an exponential term in \mathbf{Z} , that is $p(\mathbf{X}) = \int p(\mathbf{X}, \mathbf{Z}) d\mathbf{Z}$, thus rendering the overall problem described in Eq.1 intractable in the average case. Originally derived using Jensen's inequality (Jordan et al. 1999), a tractable lower bound on the evidence is revealed,

$$\begin{aligned} \log p(\mathbf{X}) - \text{KL}(q(\mathbf{Z}) \parallel p(\mathbf{Z} \mid \mathbf{X})) = \\ \mathbb{E}_q[\log p(\mathbf{X} \mid \mathbf{Z})] - \text{KL}(q(\mathbf{Z}) \parallel p(\mathbf{Z})) \end{aligned} \quad (2)$$

where the first term expresses likelihood (or reconstruction) of the data under the given parameters while the divergence terms counteracts such parameterization to adjust for the assumed prior. Choosing $p_{\phi}(\mathbf{X} \mid \mathbf{Z})$ and $q(\mathbf{Z}) := q_{\theta}(\mathbf{Z} \mid \mathbf{X})$ to be parameterized as neural networks leads to the variational auto-encoder (VAE) model class (Kingma and Welling 2019). Importance sampling (Rubinstein and Kroese 2016) reveals a connection between variational methods (VAE) and sampling techniques for performing marginal inference i.e., since

$$p(\mathbf{X}) \approx \frac{1}{n} \sum_{i=1}^n \frac{p_{\phi}(\mathbf{X} \mid \mathbf{z}_i)p(\mathbf{z}_i)}{q_{\theta}(\mathbf{z}_i \mid \mathbf{X})} \quad (3)$$

where the number of samples n is being kept moderate through the likelihood ratio induced by q .

¹Uniformly covering a unit hypercube of n dimensions with k samples scales exponentially, $O(k^n)$.

Graph Neural Networks. In geometric deep learning as portraited by (Bronstein et al. 2021), graph neural networks (GNN) constitute a fundamental class of function approximator that place an inductive bias on the structural relations of the input. A GNN layer $f(\mathbf{D}, \mathbf{A}_G)$ over some data considered to be vector-valued samples of our variables $\{\mathbf{d}_i\}_{i=1}^n \mathbf{D} \in \mathbb{R}^{d \times n}$ and an adjacency representation $\mathbf{A}_G \in [0, 1]^{d \times d}$ of a graph G is generally considered to be a permutation equivariant² application of permutation invariant functions $\phi(\mathbf{d}_X, \mathbf{D}_{\mathcal{N}_X^G})$ on each of the variables (features) \mathbf{d}_i and their respective neighborhoods within the graph \mathcal{N}_i^G . The most general form of a GNN layer is specified by

$$\mathbf{h}_i = \phi \left(\mathbf{d}_i, \bigoplus_{j \in \mathcal{N}_i^G} \psi(\mathbf{d}_i, \mathbf{d}_j) \right), \quad (4)$$

where \mathbf{h}_i represents the updated information of node i aggregated (\bigoplus) over its neighborhood in the form of messages ψ . The flavour of GNN presented in Eq.4 is being referred to as message-passing (Gilmer et al. 2017) and constitutes the most general class of GNN that supersedes both convolutional (Kipf and Welling 2016a) and attentional (Veličković et al. 2017) flavours of GNN. In the context of representation learning on graphs, GCN were previously used within a VAE pipeline as means of parameterization to the latent variable posterior $p(\mathbf{Z} \mid \mathbf{X})$ (Kipf and Welling 2016b).

Causal Inference. A Structural Causal Model (SCM) as defined by (Peters, Janzing, and Schölkopf 2017) is specified as $\mathfrak{C} := (\mathbf{S}, P(\mathbf{U}))$ where $P(\mathbf{U})$ is a product distribution over exogenous unmodelled variables and \mathbf{S} is defined to be a set of d structural equations

$$V_i := f_i(\text{pa}(V_i), U_i), \quad \text{where } i = 1, \dots, d \quad (5)$$

with $\text{pa}(V_i)$ representing the parents of variable V_i in graph $G(\mathfrak{C})$. An intervention $do(\mathbf{W})$, $\mathbf{W} \subset \mathbf{V}$ on a SCM \mathfrak{C} as defined in (5) occurs when (multiple) structural equations are being replaced through new non-parametric functions $g_{\mathbf{W}}$ thus effectively creating an alternate SCM $\mathfrak{C}_2 := \mathfrak{C}^{do(\mathbf{W}=g_{\mathbf{W}})}$. Interventions are referred to as *imperfect* if the parental relation is kept intact, $g_i(\text{pa}_i, \cdot)$, and as *atomic* if $g_i = a$ for $a \in \mathbb{R}$. An important property of interventions often referred to as "modularity" or "autonomy"³ states that interventions are fundamentally of local nature, formally

$$p^{\mathfrak{C}_1}(V_i \mid \text{pa}(V_i)) = p^{\mathfrak{C}_2}(V_i \mid \text{pa}(V_i)), \quad (6)$$

where the intervention of \mathfrak{C}_2 occurred on variable V_j opposed to V_i . This suggests that mechanisms remain invariant to changes in other mechanisms which implies that only information about the effective changes induced by the intervention need to be compensated for. An important consequence of autonomy is the truncated factorization

$$p(\mathbf{V}) = \prod_{V \notin \mathbf{W}} p(V \mid \text{pa}(V)) \quad (7)$$

²That is, for some permutation matrix $\mathbf{P} \in [0, 1]^{d \times d}$, it holds that $f(\mathbf{P}\mathbf{D}, \mathbf{P}\mathbf{A}_G\mathbf{P}^T) = \mathbf{P}f(\mathbf{D}, \mathbf{A}_G)$.

³See Section 6.6 in (Peters, Janzing, and Schölkopf 2017).

derived by (Pearl 2009), which suggests that an intervention $do(\mathbf{W})$ introduces an independence of a set of intervened nodes \mathbf{W} to its causal parents. Another important assumption in causality is that causal mechanisms do not change through intervention suggesting a notion of invariance to the cause-effect relations of variables which further implies an invariance to the origin of the mechanism i.e., whether it occurs naturally or through means of intervention (Pearl, Glymour, and Jewell 2016). A SCM \mathfrak{C} is capable of emitting various mathematical objects such as graph structure, statistical and causal quantities placing it at the heart of causal inference, rendering it applicable to machine learning applications in marketing (Hair Jr and Sarstedt 2021), healthcare (Bica, Alaa, and Van Der Schaar 2020) and education (Hoiles and Schaar 2016). A SCM induces a causal graph G , an observational/associational distribution $p^{\mathfrak{C}}$, can be intervened upon using the do -operator and thus generate interventional distributions $p^{\mathfrak{C};do(\dots)}$ and given some observations \mathbf{v} can also be queried for interventions within a system with fixed noise terms amounting to counterfactual distributions $p^{\mathfrak{C}|\mathbf{V}=\mathbf{v};do(\dots)}$. As suggested by the Causal Hierarchy Theorem (CHT) (Bareinboim et al. 2020), these properties of an SCM almost always form the Pearl Causal Hierarchy (PCH) consisting of different levels of distributions being \mathcal{L}_1 associational, \mathcal{L}_2 interventional and \mathcal{L}_3 counterfactual. This hierarchy suggests that causal quantities ($\mathcal{L}_i, i \in \{2, 3\}$) are in fact richer in information than statistical quantities (\mathcal{L}_1), and the necessity of causal information (e.g. structural knowledge) for inference based on lower rungs e.g. $\mathcal{L}_1 \not\rightarrow \mathcal{L}_2$. Finally, to query for samples of a given SCM, the structural equations are being simulated sequentially following the underlying causal structure starting from independent, exogenous variables U_i and then moving along the causal hierarchy of endogenous variables \mathbf{V} . To conclude, consider the formal definition of valuations for the first two layers being

$$p^{\mathfrak{C}}(\mathbf{y} \mid do(\mathbf{x})) = \sum_{\{\mathbf{u} \mid \mathbf{Y}_{\mathbf{x}}(\mathbf{u}) = \mathbf{y}\}} p(\mathbf{u}) \quad (8)$$

for instantiations \mathbf{x}, \mathbf{y} of the node sets $\mathbf{X}, \mathbf{Y} \subseteq \mathbf{V}$ where $\mathbf{Y}_{\mathbf{x}} : \mathbf{U} \mapsto \mathbf{Y}$ denotes the value of \mathbf{Y} under intervention \mathbf{x} .

The GNN-SCM-NCM Connection

To expand further on the boundaries of the integration between causality and machine learning, we perform a theoretical investigation on the relation between graph neural networks (GNN) and structural causal models (SCM), thereby transitively also to neural causal models (NCM). While all the established results on causal identification have proven that intervention/manipulation is not necessary for performing causal inference, the concept of intervention/manipulation still lies at the core of causality as suggested by the long-standing motto of Peter Holland and Don Rubin '*No causation without manipulation*' (Holland 1986). The centrality of interventions is why we choose to consider interventions as a starting point of our theoretical investigation. Thereby, we first define a process of intervention within the GNN computation layer that will subsequently reveal sensible properties of the process akin to those of intervention on SCM.

Definition 1. (Interventions within GNN.) An intervention \mathbf{x} on the corresponding set of variables $\mathbf{X} \subseteq \mathbf{V}$ within a GNN layer $f(\mathbf{D}, \mathbf{A}_G)$, denoted by $f(\mathbf{D}, \mathbf{A}_G \mid do(\mathbf{X} = \mathbf{x}))$, is defined as a modified layer computation,

$$\mathbf{h}_i = \phi \left(\mathbf{d}_i, \bigoplus_{j \in \mathcal{M}_i^G} \psi(\mathbf{d}_i, \mathbf{d}_j) \right), \quad (9)$$

where the intervened local neighborhood is given by

$$\mathcal{M}_i^G = \{j \mid j \in \mathcal{N}_i^G, j \notin \text{pa}_i \iff i \in \mathbf{X}\} \quad (10)$$

where \mathcal{N}^G denotes the regular graph neighborhood. A GNN layer that computes Eq.9 is said to be *interventional*.

An intervention, just like in an SCM, is of local nature. I.e., the new neighborhood of a given node is a subset of the original neighborhood at any time, $\mathcal{M} \subseteq \mathcal{N}$. The notion of intervention belongs to the causal layers of the PCH i.e., layers 2 (interventional) and 3 (counterfactual). Fig.1 presents an intuitive illustration each for both the underlying SCM with its various properties and the intervention process within the GNN layer. The motivational origin of this work lies in the tighter integration of causality with today's machine learning methodologies, more specifically neural network variants. We envision a fully-differentiable system that combines the benefits of both worlds. As a step towards this goal, we introduce the concept of intervention for GNNs (Def.1). The reader might wonder why counterfactuals (\mathcal{L}_3) are not being covered in this work. The reason for this lies in the fact that a conversion between GNN and SCM will necessarily have to cope with transforming a shared, global function ψ into the collection of all local partial mechanisms f_{ij} of any structural equation. Thereby, optimization becomes tremendously difficult. More formally, we state the following theorem on the model conversion.

Theorem 1. (GNN-SCM Conversion.) Consider the most general formulation of a message-passing GNN node computation $\mathbf{h}_i : \mathcal{F} \mapsto \mathcal{F}'$ as in Eq.4. For any SCM $\mathfrak{C} = (\mathbf{S}, P(\mathbf{U}))$ there exists always a choice of feature spaces $\mathcal{F}, \mathcal{F}'$ and shared functions ϕ, ψ , such that for all structural equations $f \in \mathbf{S}$ it holds that $\mathbf{h}_i = f_i$.

Because of space restrictions we provide the proof to Thm.1 and all subsequent mathematical results within the supplementary section. It seems that the common ground between SCM and GNN lies within the assumed graph structure and thus is deemed suitable as a starting point for a reparameterization from SCM to GNN as Thm.1 suggests. However, while Thm.1 is powerful in the sense that any GNN can be seen as a neural SCM variant, the theorem does not give away any information on optimization. It follows naturally that ψ is a *shared* function amongst all nodes of the graph while an SCM considers a specific mechanism *for each* of the nodes in the graph, and thus optimization becomes difficult. In a nutshell, the messages $\psi(i, j)$ need to model each of the dependency terms f_{ij} within a structural equation, such that the messages themselves become a descriptor of the causal relation for $(i \leftarrow j)$. Nonetheless, the theoretical connection exists, suggesting a tighter integration for neural-causal models, and an important consequence of

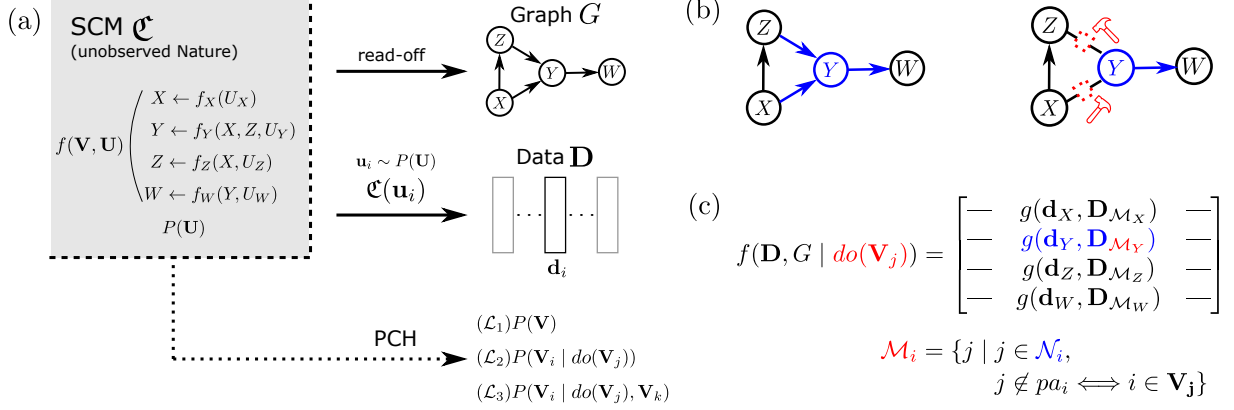


Figure 1: **Graph Neural Networks and Interventions akin to SCM.** A schematic overview. (a) shows the unobserved SCM Σ that generates data \mathbf{D} through instantiations of the exogenous variables \mathbf{U} . The SCM implies a graph structure G and the PCH (\mathcal{L}_i) (b) shows the intuition behind interventions using the do -operation (c) presents the mathematical formalism (Def.1) highlighting the intervention (red) and the regular neighborhood (blue). (Best viewed in color.)

Thm.1 is the connection to the definition of Neural Causal Models (NCM) as posed by (Xia et al. 2021).

Corollary 1. (NCM-Type 2.) *Allowing for the violation of sharedness of ψ as dictated in Thm.1 and choosing $\mathcal{F} = \mathcal{F}' = \mathbf{U} \cup \mathbf{V}$ to be the union over endo- and exogenous variables, $\phi(i, \dots) = U_i + \sum(\dots)$ to be a sum-aggregator with noise term selection, and $\psi = \{f_{\theta}^{ij}\}$ to be the dependency terms of the structural equations f_i modelled as feedforward neural networks. Then the computation layer $\{\mathbf{h}_i\}_{i=1}^{|V|}$ is a special case of the NCM as in (Xia et al. 2021).*

To be more precise, the NCM-Type 2 portraited in Cor.1 is more fine-grained than the the definition of NCM in (Xia et al. 2021) since their formulation models structural equations using feedforward nets ($|V|$) while the NCM-Type 2 models the *dependency terms within* each of the structural equations ($|\mathcal{E}^2|$). Fig.2 provides a schematic illustration of the discussed concepts, that is, both for the GNN to SCM conversion from Thm.1 and the NCM-Type 2 comparison to regular NCM from Cor.1. The decomposition in Fig.2(a) follows from (Kuo et al. 2010). On a sidenote, it is worth noting that the computation layer in Cor.1, as soon as sharedness is being violated, generally is not considered to be a GNN layer anymore since sharedness just like adjacency information and permutation-equivariance belong to key properties of the GNN definition. Nonetheless, Corr.1 predicts a new type of NCM that should be investigated in more detail in future research as it should provide the same theoretical guarantees as regular NCM, while being more flexible and interpretable because of the fine-grained modelling scope (Fig.2(b)).

GNN-based Causal Inference

To return to the main line of research of this work, the difficulty of optimization for a general model as suggested by Thm.1 (Fig.2(c)) is thereby the reason for us to focus on what is reasonably attainable within the GNN framework since the inductive bias on graphs still seems appealing. The graph-intersection of these two model classes can in fact be

(a)

$$\begin{aligned} X \leftarrow f_X(Z, U_X) &= f_{XZ}(Z) + f_{UX}(U_X) \\ Y \leftarrow f_Y(Z, X, U_Y) &= f_{YZ}(Z) + f_{YX}(X) + f_{UY}(U_Y) \\ Z \leftarrow f_Z(U_Z) &= f_{UZ}(U_Z) \end{aligned}$$

(b)

(c)

GNN \rightarrow SCM

$$V_i = \phi\left(v_i, \bigoplus_{j \in \mathcal{N}_i^G} \psi(v_i, v_j)\right)$$

$$\psi(i, j) = \begin{cases} f_{XZ}(Z), & \text{for } i = X, j = Z \\ f_{YZ}(Z), & \text{for } i = Y, j = Z \\ f_{YX}(X), & \text{for } i = Y, j = X \end{cases}$$

Figure 2: **NCM-Type 2 and the GNN-SCM Conversion.** A schematic overview of the results established in Thm.1 and Cor.1 (a) shows an example SCM as the underlying reality. Note the decomposition of the initially multivariate function f into scalar dependency terms f_{ij} (b) shows the NCM as defined by (Xia et al. 2021) which models on node-level opposed to the edge-level as for NCM-Type 2 (Cor.1) (c) shows an example of an infeasible ψ function that has to model a quadratic number of functions. (Best viewed in color.)

leveraged to partially represent the PCH as we show next. I.e., up to rung 2 of interventional queries (\mathcal{L}_2). Instead of turning a GNN into an SCM (as in Thm.1), we will consider the reverse direction. Thereby, we define a GNN construction based on an SCM.

Definition 2. (\mathfrak{G} -GNN construction.) *Let \mathfrak{G} be the graph induced by SCM Σ . A GNN layer $f(\mathbf{D}, \mathbf{A}_G)$ for which $G = \mathfrak{G}$ is said to be \mathfrak{G} -constructed.*

We believe that \mathfrak{G} -GNN (Def.2) make an important step towards connecting the graph structure induced by an SCM with the structured computation within a GNN layer. Developing further on this notion in future research might allow for neural-graph models that are inherently causal⁴.

⁴Consider (Xia et al. 2021) for a recent treatise on Neural

Proposition 1. (Graph Mutilation Equivalence.) Let \mathfrak{C} be an SCM with graph \mathfrak{G} and let f be a \mathfrak{G} -GNN layer. An intervention $do(\mathbf{X})$, $\mathbf{X} \subseteq V$, on both \mathfrak{C} and f produces the same mutilated graph \mathfrak{G}' .

It is worth noting that an intervention within a GNN layer (Def.1) is dual to the notion of intervention within an SCM i.e., like observing within the mutilated graph is akin to interventions, computing a regular GNN layer on the mutilated graph is akin to intervening on the original GNN layer, that is, $f(\mathbf{D}, \mathbf{A}_G | do(\mathbf{X})) = f(\mathbf{D}, \mathbf{A}_{G'})$ where G' is the graph upon intervention $do(\mathbf{X})$. In the spirit of (Xia et al. 2021), we define what it means for an SCM to be consistent with another causal model in terms of the PCH layers \mathcal{L}_i .

Definition 3. (Partial \mathcal{L}_i -Consistency.) Consider a model \mathcal{M} capable of partially emitting PCH, that is \mathcal{L}_i for $i \in \{1, 2\}$, and an SCM \mathfrak{C} . \mathcal{M} is said to be partially \mathcal{L}_i -consistent w.r.t. \mathfrak{C} if $\mathcal{L}_i(\mathcal{M}) \subset \mathcal{L}_i(\mathfrak{C})$ with $|\mathcal{L}_i(\mathcal{M})| > 0$.

In the following we will usually omit the word partial since Def.3 is the only consistency employed. A causal model most generally defined can be considered to be something that can carry out causal inferences and in Def.3 we consider such models that are capable of emitting the \mathcal{L}_i -distributions. The definition proposes that an SCM can match with such a model, if it agrees on a subset of all conceivable distributions for a level i , which for $|\mathcal{L}_1| = 1$ but $|\mathcal{L}_2| \rightarrow \infty$. In their work on variational graph auto-encoders (VGAE) (Kipf and Welling 2016b) considered the application of the GNN model class to the posterior parameterization, $q(\mathbf{Z} | \mathbf{D}, \mathbf{A}) = f(\mathbf{D}, \mathbf{A})$. However, their main incentive posed to be a generative model on graphs themselves i.e., $p(\mathbf{A} | \mathbf{Z})$. In the following, we define VGAE on the original data as traditionally done within vanilla VAE models that don't consider (or ignore) structured input.

Definition 4. (Variational Graph Auto-Encoder.) We define a VGAE $\mathcal{V} = (q(\mathbf{Z} | \mathbf{D}), p(\mathbf{D} | \mathbf{Z}))$, as a data-generative model, with inference and generator model respectively such that $q := f_{\theta}(\mathbf{D}, \mathbf{A})$ is a GNN layer and $p := g_{\phi}(\mathbf{D}, \mathbf{Z})$ some parameterized data \mathbf{D} dependent model, where θ, ϕ are the variational parameters.

Since SCM induce a graph structure dictated by the set of structural equations that implicitly govern the structural relations between the modelled variables, it is important to define a density estimator which acts on the variable space opposed to the space of plausible graph structures (Def.4). Using a GNN layer for modelling the original data does not compromise on the expressiveness of the model class as following theorem suggests.

Theorem 2. (Universal Density Approximation.) There exists a latent variable family q and a corresponding data-generative VGAE $\mathcal{V} = (q, p)$ such that the modelled density can approximate any smooth density at any nonzero error.

This theorem suggests that the defined VGAE class, for a suitable choice of latent variable model, is a universal approximator of densities (UDA). A suitable choice for

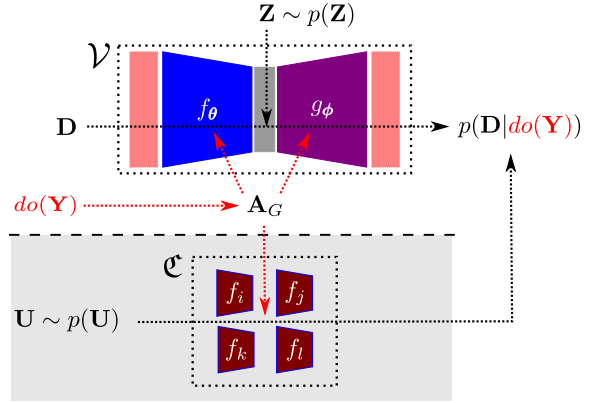


Figure 3: Neural-Causal Model based on Interventional GNN Layers. A schematic overview of the inference process within the neural-causal iVGAE \mathcal{V} model and its similarities to the same process within an SCM \mathfrak{C} . While \mathfrak{C} can be directly queried for the causal effect $p(\mathbf{D} | do(\mathbf{Y}))$ through valuations \mathbf{U} , the iVGAE makes use of corresponding data \mathbf{D} . (Best viewed in color.)

q in Thm.2 is the mixture of Gaussians family (Goodfellow, Shlens, and Szegedy 2015; Plataniotis and Hatzinakos 2017). Since causal estimates are determined by their theoretical identifiability from the partially available information on the true underlying SCM \mathfrak{C}^* (e.g. structural constraints), UDA properties of the estimator are beneficial. Since the data-generative VGAE is a probabilistic model capable of approximating distributions to arbitrary precision, we are finally ready to define a causal model based on GNN layers by introducing *interventional GNN layers* (Def.1) into said VGAE class.

Definition 5. (Interventional VGAE.) An *interventional VGAE* is a data-generative VGAE $\mathcal{V} = (q, p)$ where both q, p are set to be *interventional GNN layers* $f_i(\mathcal{D}, \mathbf{A}_G | do(\mathbf{X}))$ where $\mathcal{D} = \{\mathbf{D}, \mathbf{Z}\}$ respectively.

While the reader might expect the data-generative VAE model to make use of the interventions within GNN layers from Def.1, what might come as surprise is the usage of a second (interventional) GNN layer as decoder because the second layer parameterization considers the reverse module $p(\cdot | \mathbf{Z})$ which takes the latent variable \mathbf{Z} which only transitively via \mathbf{D} acquires its connection to the adjacency \mathbf{A}_G . Interventional capability within both models is beneficial since the knowledge on the specific mutilation becomes available throughout the complete model. Modified decoder that leverage pre-defined inductive biases have been deployed in the literature by for instance (Kipf et al. 2018). Fig.3 illustrates this intuition and parallels it with the computation within an SCM. The interventional VGAE (iVGAE) is a causal model, like an SCM, capable of emitting \mathcal{L}_i -distributions from the PCH. With this, we are able to provide statements on the causal capabilities of this extended model class. More precisely, following the mathematical ideas of (Xia et al. 2021) we show that iVGAE overlap with the space of all SCMs Ω .

Theorem 3. (Expressivity.) For any SCM \mathfrak{C} there exists an iVGAe $\mathcal{V}(\theta, \phi)$ for which \mathcal{V} is \mathcal{L}_2 -consistent w.r.t \mathfrak{C} .

Similar to the peculiar specifications of NCM (Xia et al. 2021), an iVGAe does not loose in expressivity to SCM regarding the first two rungs of the PCH. Thus it can also act as a proxy for causal inferences. An important consequence of the CHT (Bareinboim et al. 2020), which also applies to iVGAe is that the PCH is kept in tact across scenarios.

Corollary 2. (iVGAe Partial Causal Hierarchy Theorem.) Consider the sets of all SCM and iVGAe, Ω, Υ , respectively. If for all $\mathcal{V} \in \Upsilon$ it holds that \mathcal{V} is $\mathcal{L}_1^p(\mathcal{V}) = \mathcal{L}_1^p(\mathfrak{C}) \implies \mathcal{L}_2^q(\mathcal{V}) = \mathcal{L}_2^q(\mathfrak{C})$ with $\mathfrak{C} \in \Omega$, where $\mathcal{L}_i^p \subset \mathcal{L}_i$ is a selection p, q over the set of all level 1,2 distributions respectively, then we say that layer 2 of iVGAe collapses relative to \mathfrak{C} . On the Lebesgue measure over SCMs, the subset in which layer 2 of iVGAe collapses to layer 1 has measure zero.

As previously pointed out by (Xia et al. 2021; Bareinboim et al. 2020), the CHT does not impose a negative result by claiming impossibility on low-to-high-layer inferences, however, it suggests that even sufficient expressivity of a model does not allow for the model to overcome the boundaries of the layers (unless causal information e.g. in the form of structural constraints is available). Another noteworthy consequence of both Thms.3 and 1 is the incapability of handling counterfactuals.

Corollary 3. (iVGAe Limitation.) For any SCM \mathfrak{C} there exists no iVGAe \mathcal{V} such that \mathcal{V} is \mathcal{L}_3 -consistent w.r.t. \mathfrak{C} .

While the formulation of an iVGAe restricts itself from the full expressivity of the PCH (like SCM or NCM), there are no restrictions on the lower causal layers in addition to a more compact overall model. In Def.2 we pointed to the relation between SCM and GNN via the deployed graph. The following theorem states that if \mathfrak{G} -GNN layers are being deployed within a corresponding VGAE, then we can have consistency to any SCM of choice.

Corollary 4. (\mathcal{L}_2 Representation.) For any SCM \mathfrak{C} that induces a graph \mathfrak{G} , there exists a corresponding iVGAe $\mathcal{V} = (q, p)$ where q, p are \mathfrak{G} -GNN layers such that \mathcal{V} is \mathcal{L}_2 -consistent with \mathfrak{C} .

The main claim of this theorem is two-fold, first, that the expressivity established in Thm.3 is being preserved for \mathfrak{G} -GNN layers, and second, that GNN and SCM allow for a tighter integration through the shared graph \mathfrak{G} .

Identifiability and Estimation

In line with (Xia et al. 2021), we finally set stage for identifiability within the neural-causal iVGAe model by first extending their notion of neural identifiability, since iVGAe is a neural model that makes trades the set of feedforwards networks for two interventional graph neural networks.

Definition 6. (Neural Identifiability.) Again, let Ω, Υ be the sets of SCMs and corresponding \mathfrak{G} -GNN based iVGAe. For any pair $(\mathfrak{C}, \mathcal{V}) \in \Omega \times \Upsilon$, a causal effect $p(\mathbf{V}_i | do(\mathbf{V}_j))$ is called neurally identifiable iff the pair agrees on both the causal effect $[p^{\mathfrak{C}}(\mathbf{V}_i | do(\mathbf{V}_j)) = p^{\mathcal{V}}(\mathbf{V}_i | do(\mathbf{V}_j))]$ and the observational distributions $[p^{\mathfrak{C}}(\mathbf{V}) = p^{\mathcal{V}}(\mathbf{V})]$.

Algorithm 1: Causal Inference with GNN

Input: iVGAe modules \mathcal{V}_i , Intervention \mathbf{v}_j , Variable \mathbf{v}_i
Parameter: Number of Samples n
Output: $\log(\hat{p}(\mathbf{v}_i | do(\mathbf{V}_j = \mathbf{v}_j)))$

- 1: Let $\log(\hat{p}(\mathbf{v}_i | do(\mathbf{V}_j = \mathbf{v}_j))) = 0$ and $i = 0$
- 2: **while** $i \leq n$ **do**
- 3: Encoding \mathbf{z} , $\log(p(\mathbf{z} | do(\mathbf{v}_j))) \leftarrow \mathcal{V}_1(\mathbf{v}_i, \mathbf{v}_j)$
- 4: Decoding $\log(p(\mathbf{v}_i | \mathbf{z} do(\mathbf{v}_j))) \leftarrow \mathcal{V}_2(\mathbf{z}, \mathbf{v}_i, \mathbf{v}_j)$
- 5: Aggregate $\hat{p} \leftarrow \exp(\log(p(\mathbf{v}_i | \mathbf{z} do(\mathbf{v}_j))) - \dots - \log(p(\mathbf{z} do(\mathbf{v}_j))))$
- 6: $i \leftarrow i + 1$
- 7: **end while**
- 8: **return** $\log(\hat{p}) - \log(n)$

This definition enforces a matching on all the relevant levels such that a causal effect becomes identifiable. With this, a final central claim on the relation of general identifiable effects and neurally identifiable effects (i.e., using the iVGAe as the model of choice) is being established.

Theorem 4. (Dual Identification.) Consider the causal quantity of interest $Q = p^{\mathfrak{C}}(\mathbf{V}_i | do(\mathbf{V}_j))$, \mathfrak{G} the true causal graph underlying SCM $\mathfrak{C} \in \Omega$ and $p(\mathbf{V})$ the observational distribution. Q is neurally identifiable from iVGAe $\mathcal{V} \in \Upsilon$ with \mathfrak{G} -GNN modules iff Q is identifiable from \mathfrak{G} and $p(\mathbf{V})$.

This theorem is analouge to the statement on neural identifiability in (Xia et al. 2021) thus following the same implications in that theoretically lower-to-higher-layer inference is possible within our neural setting, avoiding the usage of *do*-calculus altogether. The hope lies within the differentiability of the considered (neural) models to allow for leveraging causal inferences automatically from large-scale data. From a causal perspective, it is important to note that Def.6 alongside the theoretical result Thm.4 consider identifiability and not actual identification, the former refers to the power of cross-layer inferences while the latter refers to the process of using e.g. *do*-calculus for SCM or mutilation in the case of NCM to obtain the estimands⁵. For the iVGAe identification thus refers to cross-layer modelling which is a special case of multi-layer modelling, to which we will simply refer to as estimation. The estimation is performed using a modified version of the variational objective in Eq.2 to respect the causal quantities,

$$\mathbb{E}_q[\log p(\mathbf{V} | \mathbf{Z}, do(\mathbf{W}))] - \text{KL}(q(\mathbf{Z} | do(\mathbf{W})) || p(\mathbf{Z})), \quad (11)$$

where $\mathbf{W} \subset \mathbf{V}$ are intervened variables and p, q the \mathfrak{G} -GNNs of the iVGAe model. After optimizing the iVGAe model with Eq.11, we can consider any quantity of interest dependent on the modelled levels $Q(\mathcal{L}_i)$. One interesting choice for Q is the average treatment effect (ATE),

$$\text{ATE}(X, Y) := \mathbb{E}[Y | do(X=1)] - \mathbb{E}[Y | do(X=0)], \quad (12)$$

where the binary⁶ variable X is being referred to as treatment. In addition to estimation one can consider classification on identifiable structures. In Alg.1 we show how

⁵These estimands can then be estimated using data.

⁶Note that we can extend Eq.12 to be categorical/continuous.

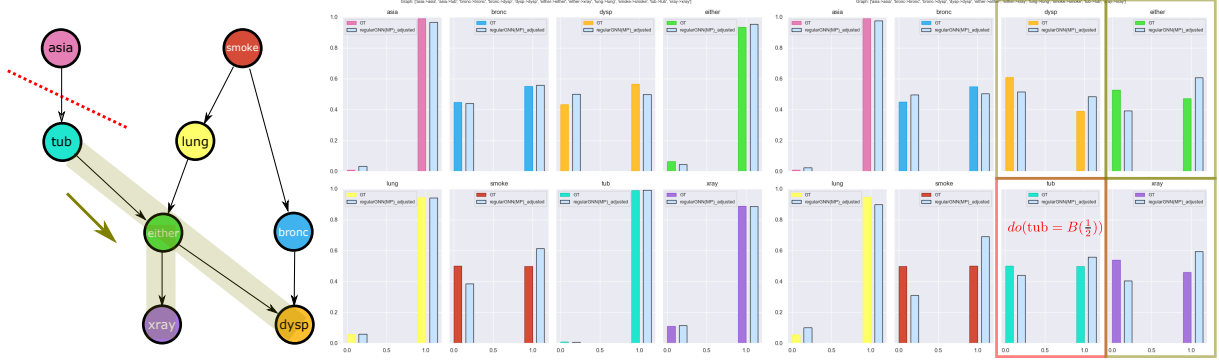


Figure 4: **GNN Capture Causal Influence.** An illustration of causal density estimation (left \mathcal{L}_1 , right \mathcal{L}_2 using Alg.1 on the ASIA data set. The intervention $do(tub = B(\frac{1}{2}))$ turns the property 'tub' into a fair coin flip (red box) causally influences its descendants (olive boxes). iVGAE (lightblue bars) adequately reacts to the distributional changes. (Best viewed in color.)

marginal inference under intervention is being performed using importance sampling. Since we consider the Markovian case, all structures become identifiable with the knowledge on the corresponding causal graph \mathfrak{G} . However, due to the way optimization behaves in practice, a similar classification to NCM is interesting for further inspection. In NCM one can define a threshold-based classification measure for identification. We consider similarly different thresholds to evaluate whether an estimation is sufficiently close to the identification quantity of interest. Mathematically, in this test formulation, a quantity has been correctly identified if the iVGAE \mathcal{V} can model the selected distributions p of the family of SCMs $\mathfrak{F}_G = \{\mathfrak{C} \mid \mathfrak{C} \models G\}$, that all model the same structure G at the second-level of the PCH, sufficiently well according to a threshold $\tau \in \mathbb{R}$, that is $|\mathcal{L}_2^p(\mathcal{V}) - \mathcal{L}_2^p(\mathfrak{F})| < \tau$.

Empirical Illustration

To assist our theoretical results we provide an empirical illustration. Due to space constraints, we only highlight relevant key results while pointing to the [extensive Appendix](#).

Causal Effect Estimation and Identification. We investigate the estimation of the ATE (Def.12) and identification using iVGAE (Def.5) on different families of SCMs, that is, different structures with different parameterizations. Estimation considers the predictive quality amongst different parameterizations, while identification considers a structure independent of parameterizations. In Fig.5 chain and backdoor structures are being shown. For the chain, both estimation/identification generally improve with an increase in data exposure. The ATE is strictly positive. For the backdoor, the ATE can take on any value depending on the parameterization, and this reflects in terms of both estimation/identification. An extensive study is provided in the Appendix.

Density Estimation. We investigate properties of the causal density estimation when using iVGAE (Def.5). We inspect various aspects like for instance how interventional influence propagates along the topological sequence or how precisely the model is able to fit. Fig.4 shows an iVGAE model on the real-world inspired ASIA data set (Lauritzen

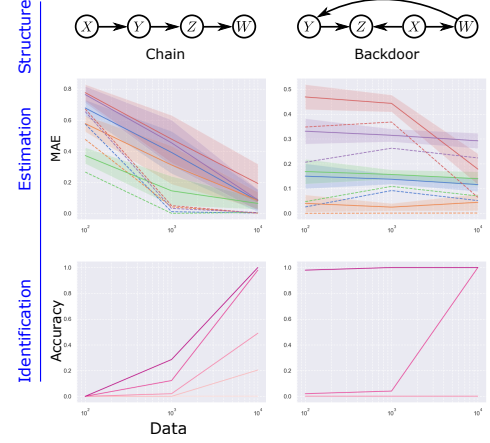


Figure 5: **Estimation and Identification.** Please consider the remainder in the Appendix. Two SCM structures (top row), the mean absolute error on the ATE (middle row) and identification accuracy (bottom row). (Best viewed in color.)

and Spiegelhalter 1988) that estimates the observational and interventional distributions from data sufficiently well in terms of both quality and recall. Inference is performed using Alg.1. An extensive study is provided in the Appendix.

Conclusions and Future Work

We derive the first theoretical connection between GNNs and SCMs (Thm.1) from first principles and in the process extend the family of neural causal models with two new classes: NCM-Type 2 (Cor.1) and iVGAE (Def.5). We provide several theoretical results on the feasibility, expressivity and identifiability (Thms.3,4; Cors.3,4). To support the theoretical results empirically, we systematically investigate practical causal inference on several benchmarks. Following, an extension that supports the complete PCH without feasibility trade-off would be desirable. Differently encoding the intervention within GNN (Def.1) or concepts like PMP (Strathmann et al. 2021) might allow for this direction. Further, testing on larger causal systems is a next step.

References

Bareinboim, E.; Correa, J. D.; Ibeling, D.; and Icard, T. 2020. 1On Pearl’s Hierarchy and.

Bica, I.; Alaa, A.; and Van Der Schaar, M. 2020. Time series deconfounder: Estimating treatment effects over time in the presence of hidden confounders. In *ICML*.

Blei, D. M.; Kucukelbir, A.; and McAuliffe, J. D. 2017. Variational inference: A review for statisticians. *Journal of the American statistical Association*, 112(518): 859–877.

Bronstein, M. M.; Bruna, J.; Cohen, T.; and Veličković, P. 2021. Geometric deep learning: Grids, groups, graphs, geodesics, and gauges. *arXiv preprint arXiv:2104.13478*.

Bronstein, M. M.; Bruna, J.; LeCun, Y.; Szlam, A.; and Vandergheynst, P. 2017. Geometric deep learning: going beyond euclidean data. *IEEE Signal Processing Magazine*, 34(4): 18–42.

Buchsbaum, D.; Bridgers, S.; Skolnick Weisberg, D.; and Gopnik, A. 2012. The power of possibility: Causal learning, counterfactual reasoning, and pretend play. *Philosophical Transactions of the Royal Society B: Biological Sciences*, 367(1599): 2202–2212.

Cybenko, G. 1989. Approximation by superpositions of a sigmoidal function. *Mathematics of control, signals and systems*, 2(4): 303–314.

Derrow-Pinion, A.; She, J.; Wong, D.; Lange, O.; Hester, T.; Perez, L.; Nunkesser, M.; Lee, S.; Guo, X.; Wiltshire, B.; et al. 2021. ETA Prediction with Graph Neural Networks in Google Maps. *CIKM*.

Gilmer, J.; Schoenholz, S. S.; Riley, P. F.; Vinyals, O.; and Dahl, G. E. 2017. Neural message passing for quantum chemistry. In *International conference on machine learning*, 1263–1272. PMLR.

Gondal, M. W.; Wüthrich, M.; Miladinović, D.; Locatello, F.; Breidt, M.; Volchkov, V.; Akpo, J.; Bachem, O.; Schölkopf, B.; and Bauer, S. 2019. On the transfer of inductive bias from simulation to the real world: a new disentanglement dataset. *arXiv preprint arXiv:1906.03292*.

Goodfellow, I.; Bengio, Y.; and Courville, A. 2016. *Deep learning*. MIT press.

Goodfellow, I. J.; Shlens, J.; and Szegedy, C. 2015. Explaining and harnessing adversarial examples. *ICLR*.

Gopnik, A. 2012. Scientific thinking in young children: Theoretical advances, empirical research, and policy implications. *Science*, 337(6102): 1623–1627.

Hair Jr, J. F.; and Sarstedt, M. 2021. Data, measurement, and causal inferences in machine learning: opportunities and challenges for marketing. *Journal of Marketing Theory and Practice*.

Hinton, G.; Srivastava, N.; and Swersky, K. 2012. Neural networks for machine learning lecture 6a overview of mini-batch gradient descent. *Cited on*, 14(8): 2.

Hoiles, W.; and Schaar, M. 2016. Bounded off-policy evaluation with missing data for course recommendation and curriculum design. In *ICML*.

Holland, P. W. 1986. Statistics and causal inference. *Journal of the American statistical Association*, 81(396): 945–960.

Hornik, K. 1991. Approximation capabilities of multilayer feedforward networks. *Neural networks*, 4(2): 251–257.

Hornik, K.; Stinchcombe, M.; and White, H. 1989. Multilayer feedforward networks are universal approximators. *Neural networks*, 2(5): 359–366.

Jordan, M. I.; Ghahramani, Z.; Jaakkola, T. S.; and Saul, L. K. 1999. An introduction to variational methods for graphical models. *Machine learning*, 37(2): 183–233.

Kingma, D. P.; and Welling, M. 2019. An introduction to variational autoencoders. *arXiv preprint arXiv:1906.02691*.

Kipf, T.; Fetaya, E.; Wang, K.-C.; Welling, M.; and Zemel, R. 2018. Neural relational inference for interacting systems. In *International Conference on Machine Learning*, 2688–2697. PMLR.

Kipf, T. N.; and Welling, M. 2016a. Semi-supervised classification with graph convolutional networks. *arXiv preprint arXiv:1609.02907*.

Kipf, T. N.; and Welling, M. 2016b. Variational graph auto-encoders. *arXiv preprint arXiv:1611.07308*.

Koller, D.; and Friedman, N. 2009. *Probabilistic graphical models: principles and techniques*. MIT press.

Korb, K. B.; and Nicholson, A. E. 2010. *Bayesian artificial intelligence*. CRC press.

Krizhevsky, A.; Sutskever, I.; and Hinton, G. E. 2012. Imagenet classification with deep convolutional neural networks. *Advances in neural information processing systems*, 25: 1097–1105.

Kuo, F.; Sloan, I.; Wasilkowski, G.; and Woźniakowski, H. 2010. On decompositions of multivariate functions. *Mathematics of computation*, 79(270): 953–966.

Lauritzen, S. L.; and Spiegelhalter, D. J. 1988. Local computations with probabilities on graphical structures and their application to expert systems. *Journal of the Royal Statistical Society: Series B (Methodological)*, 50(2): 157–194.

McCarthy, J. 1998. What is artificial intelligence?

McCarthy, J.; and Hayes, P. J. 1981. Some philosophical problems from the standpoint of artificial intelligence. In *Readings in artificial intelligence*, 431–450. Elsevier.

Mitrovic, J.; McWilliams, B.; Walker, J.; Buesing, L.; and Blundell, C. 2020. Representation learning via invariant causal mechanisms. *arXiv preprint arXiv:2010.07922*.

Mnih, V.; Kavukcuoglu, K.; Silver, D.; Graves, A.; Antonoglou, I.; Wierstra, D.; and Riedmiller, M. 2013. Playing atari with deep reinforcement learning. *arXiv preprint arXiv:1312.5602*.

Pawlowski, N.; Castro, D. C.; and Glocker, B. 2020. Deep structural causal models for tractable counterfactual inference. *arXiv preprint arXiv:2006.06485*.

Pearl, J. 2009. *Causality*. Cambridge university press.

Pearl, J.; Glymour, M.; and Jewell, N. P. 2016. *Causal inference in statistics: A primer*. John Wiley & Sons.

Pearl, J.; and Mackenzie, D. 2018. *The book of why: the new science of cause and effect*. Basic books.

Penn, D. C.; and Povinelli, D. J. 2007. Causal cognition in human and nonhuman animals: A comparative, critical review. *Annu. Rev. Psychol.*, 58: 97–118.

Peters, J.; Janzing, D.; and Schölkopf, B. 2017. *Elements of causal inference*. The MIT Press.

Plataniotis, K. N.; and Hatzinakos, D. 2017. Gaussian mixtures and their applications to signal processing. In *Advanced signal processing handbook*, 89–124. CRC Press.

Rubinstein, R. Y.; and Kroese, D. P. 2016. *Simulation and the Monte Carlo method*, volume 10. John Wiley & Sons.

Steinruecken, C.; Smith, E.; Janz, D.; Lloyd, J.; and Ghahramani, Z. 2019. The automatic statistician. In *Automated Machine Learning*, 161–173. Springer, Cham.

Stokes, J. M.; Yang, K.; Swanson, K.; Jin, W.; Cubillos-Ruiz, A.; Donghia, N. M.; MacNair, C. R.; French, S.; Carfrae, L. A.; Bloom-Ackermann, Z.; et al. 2020. A deep learning approach to antibiotic discovery. *Cell*, 180(4): 688–702.

Strathmann, H.; Barekatain, M.; Blundell, C.; and Veličković, P. 2021. Persistent Message Passing. *arXiv preprint arXiv:2103.01043*.

Vaswani, A.; Shazeer, N.; Parmar, N.; Uszkoreit, J.; Jones, L.; Gomez, A. N.; Kaiser, L.; and Polosukhin, I. 2017. Attention is All you Need. In *NeurIPS*.

Veličković, P.; Cucurull, G.; Casanova, A.; Romero, A.; Lio, P.; and Bengio, Y. 2017. Graph attention networks. *arXiv preprint arXiv:1710.10903*.

Wiener, N. 1932. Tauberian theorems. *Annals of mathematics*, 1–100.

Xia, K.; Lee, K.-Z.; Bengio, Y.; and Bareinboim, E. 2021. The Causal-Neural Connection: Expressiveness, Learnability, and Inference.

Appendix - Relating Graph Neural Networks to Structural Causal Models

We make use of this appendix following the main paper to provide the proofs to the main theorems, propositions and corollaries in addition to systematic investigations regarding practical causal inference in terms of causal effect estimation, identification and general density estimation.

Proofs

This section provides all the proofs for the mathematical results established in the main paper.

Proofs for Theorem 1 and Corollary 1

While Thm.1 does not talk about optimization and feasibility, still it suggests that indeed GNN can be converted into SCM by suggesting that there always exists at least one construction of such. In the following we prove the theorem by giving a general construction scheme.

Theorem 1. (GNN-SCM Conversion.) Consider the most general formulation of a message-passing GNN node computation $\mathbf{h}_i: \mathcal{F} \mapsto \mathcal{F}'$ as in Eq.4. For any SCM $\mathfrak{C} = (\mathbf{S}, P(\mathbf{U}))$ there exists always a choice of feature spaces $\mathcal{F}, \mathcal{F}'$ and shared functions ϕ, ψ , such that for all structural equations $f \in \mathbf{S}$ it holds that $\mathbf{h}_i = f_i$.

Proof. It is sufficient to provide a general construction scheme on SCMs. Therefore, let $\mathfrak{C} = (\mathbf{S}, P(\mathbf{U}))$ be any SCM. Let $f_i(\text{pa}(i), U_i) = \sum_{j \in \text{pa}(i) \cup U_i} f_{ij}(V_j)$ be a structural equation ($f_i \in \mathbf{S}$) and its scalar-decomposition following Thm.1 in (Kuo et al. 2010). We choose the following mapping for the respective GNN computation components:

$$\mathcal{F} = \mathbf{V} \cup \mathbf{U} = \mathcal{F}' \quad (13)$$

$$\phi(i, \dots) = U_i + \sum \dots \quad (14)$$

$$\psi(i, j) = f_{ij} \quad (15)$$

where \oplus represents an argument list. Finally, it holds that

$$\begin{aligned} \mathbf{h}_i &= \phi\left(\mathbf{d}_i, \bigoplus_{j \in \mathcal{N}_i^G} \psi(\mathbf{d}_i, \mathbf{d}_j)\right) \\ &= U_i + \sum_{j \in \text{pa}(i)} f_{ij}(V_j) = f_i. \end{aligned} \quad (16)$$

□

A simple deduction of Thm.1 in which we allow for the violation of sharedness, which lies at the core of the GNN formulation, leads to the formulation of a more fine-grained NCM model than what has been defined by (Xia et al. 2021). It is more fine-grained in that this NCM-Type 2 operates on the edge-level opposed to the node-level as for regular NCM.

Corollary 1. (NCM-Type 2.) Allowing for the violation of sharedness of ψ as dictated in Thm.1 and choosing $\mathcal{F} = \mathcal{F}' = \mathbf{U} \cup \mathbf{V}$ to be the union over endo- and exogenous variables, $\phi(i, \dots) = U_i + \sum(\dots)$ to be a sum-aggregator with noise term selection, and $\psi = \{f_{\theta}^{ij}\}$ to be the dependency terms of the structural equations f_i modelled as feedforward

neural networks. Then the computation layer $\{\mathbf{h}_i\}_i^{|V|}$ is a special case of the NCM as in (Xia et al. 2021).

Proof. The proposed computation layer (NCM-Type 2) is a special case in the way it specifies the function approximators and in that it covers non-Markovianity i.e., no hidden confounding or relations on the noise terms. A NCM \mathfrak{N} is specified the same way as an SCM \mathfrak{C} with the difference being that the noise terms being uniformly distributed over the intervall $[0, 1]$, that is $U \sim \text{Unif}(0, 1)$, and the structural equations being parameterized by feedforward neural networks $f_i := \text{MLP}_i^{\theta}$ with learnable parameters θ . (Kuo et al. 2010) suggests we know that $f_i = \sum_{j \in \text{pa}(i) \cup U_i} f_{ij}(V_j)$. Furthermore, we know that $\text{MLP}_i^{\theta} = \sum_k \text{MLP}_k^{\theta_k}$ (Hornik, Stinchcombe, and White 1989). Thereby, we have that

$$\mathbf{h}_i = \sum_j f_{ij}(V_j) = \sum_j \text{MLP}_j^{\theta_j} = \text{MLP}_i^{\theta} = f_i \quad (17)$$

where $i \in \{1 \dots |V|\}$ and $j \in \text{pa}(i) \cup U_i$. □

Proof for Proposition 1

Prop.1 reassures that the established connection between SCM and GNN based on the graph that is being induced by the former is natural. More specifically, an intervention within such a \mathfrak{G} -GNN will produce the same mutilated graph as an intervention within the SCM.

Proposition 1. (Graph Mutilation Equivalence.) Let \mathfrak{C} be an SCM with graph \mathfrak{G} and let f be a \mathfrak{G} -GNN layer. An intervention $do(\mathbf{X})$, $\mathbf{X} \subseteq V$, on both \mathfrak{C} and f produces the same mutilated graph \mathfrak{G}' .

Proof. Following Def.3 in (Bareinboim et al. 2020), an interventional SCM $\mathfrak{C}_{\mathbf{x}}$ is a submodel of the original SCM \mathfrak{C} where the structural equations for variables \mathbf{X} are being replaced by the assignment \mathbf{x} . Through this operation, denoted by $do(\mathbf{X} = \mathbf{x})$, the dependency between the causal parents of any node $V_i \in \mathbf{X}$ is being lifted (as long as the assignment \mathbf{x} is not dependent on the parents). Therefore the mutilated graph is given by $\mathfrak{G}_{\mathbf{x}} = (\mathbf{V}, \mathfrak{G}^E \setminus \{(j, i) \mid V_j \in \text{pa}_i, V_i \in \mathbf{X}\})$ where \mathfrak{G}^E denotes the edge list of the original graph. Intervening on a \mathfrak{G} -GNN layer implicitly considers a modified neighborhood $\mathcal{M}_i^G = \{j \mid j \in \mathcal{N}_i^G, j \notin \text{pa}_i \iff i \in \mathbf{X}\}$ which removes exactly the relations to the parents. Since $G = \mathfrak{G}$, the mutilated graphs are the same. □

Proof for Theorem 2

Thm.2 suggests a long standing result on universal approximators for densities (Goodfellow, Bengio, and Courville 2016; Plataniotis and Hatzinakos 2017) but applied to the data-driven VGAE. Thus the proof follows analogously.

Theorem 2. (Universal Density Approximation.) There exists a latent variable family q and a corresponding data-generative VGAE $\mathcal{V} = (q, p)$ such that the modelled density can approximate any smooth density at any nonzero error.

Proof. It is sufficient for the proof to show one example of a suitable family, that is encodable by a data-driven VGAE

(Def.4) and that can act as a universal approximator of densities. Let's inspect the Gaussian Mixture Model family of latent variable models. We will use Wiener's approximation theorem (Wiener 1932) and knowledge delta functions of positive type. A delta family of positive type is defined under following conditions

1. $\int_{-a}^a \delta_\lambda(x) dx \rightarrow \lambda$ as $\lambda \rightarrow \lambda_0$ for some a .
2. For every constant $\gamma > 0$, δ_λ tends to zero uniformly for $\gamma \leq |x| \leq \infty$ as $\lambda \rightarrow \lambda_0$.
3. $\delta_\lambda(x) \geq 0$ for all x and λ .

and if it additionally satisfies $\int_{-\infty}^{\infty} \delta_\lambda(x) dx = 1$, then such a function defines a probability density for all λ . A Gaussian density is delta in the zero limit of its variance. The sequence $p_\lambda(x)$ formed by the convolution of the delta function δ_λ and an arbitrary density function p can be expressed in terms of Gaussian. Thus,

$$\begin{aligned} p_\lambda(x) &= \int_{-\infty}^{\infty} \delta_\lambda(x-u)p(u) du \\ &= \int_{-\infty}^{\infty} \mathcal{N}_\lambda(x-u)p(u) du, \end{aligned} \quad (18)$$

forms the basis for the sum of Gaussians. It follows that $p_\lambda(x)$ can in fact be approximated with a Riemann sum $p_\lambda(x) = \frac{1}{k} \sum_{i=1}^n \mathcal{N}_\lambda(x - x_i)[\xi_i - \xi_{i-1}]$ on some interval (a, b) with interval-boundary points $\xi_i, \xi_0 = a, \xi_n = b$. It follows that we can express $p_{\lambda,n}(x)$ as a convex combination of different variance Gaussians. Finally, the sought density can be expressed as

$$p(x) = \sum_{i=1}^k w_i \mathcal{N}(x; \mu_i, \Sigma) \quad (19)$$

with $\sum w_i = 1$ and $w_i \geq 0, \forall i$. Note that $x = \mathbf{x} \in \mathbb{R}^d$ holds for all the previously established results. Thus a GMM can approximate any density. To conclude, a GMM can be modelled by data-driven VGAE by designing the output of the encoder $f_\theta(\mathbf{D}, \mathbf{A}) = \mathbf{Z}$ such that $\mathbf{z}_i := w_i, \mu_i, \Sigma_i$. \square

Proofs for Theorem 3 and Corollaries 2 and 3

The iVGAE is a feasible model opposed to the GNN-reparameterization from Thm.1 for the price of expressivity. Nonetheless, the following Thm.3 reassures that the iVGAE can model causal quantites up to the second level of the PCH, namely that of interventions (\mathcal{L}_2).

Theorem 3. (Expressivity.) For any SCM \mathfrak{C} there exists an iVGAE $\mathcal{V}(\theta, \phi)$ for which \mathcal{V} is \mathcal{L}_2 -consistent w.r.t \mathfrak{C} .

Proof. Let $\mathcal{V}(\theta, \phi)$ be an iVGAE and $\mathbf{D} = \{\mathbf{d}_i\}_{i=1}^{|\mathbf{V}|}$ a data set on the variables \mathbf{V} of an arbitrary SCM \mathfrak{C} for multiple interventions of said SCM, that is, $\mathbf{d}_i \sim p_k \in \mathcal{L}_j(\mathfrak{C})$ for $j \in \{1, 2\}$ and $k > 1$. Note that the observational case (\mathcal{L}_1) is considered to be an intervention on the empty set, $p(\mathbf{V} | do(\emptyset)) = p(\mathbf{V})$. Through Thm.2 we know that there always exists a parameterization θ, ϕ for \mathcal{V} such that any distribution p can be modelled to an arbitrary precision, thus $p^{\mathcal{V}} = p_k$. Since $k > 1$ we have that \mathcal{V} models the PCH up to

level partially $\mathcal{L}_2(\mathcal{V})$. Finally, the distributions are modelled relative to \mathfrak{C} and $\mathcal{L}_2(\mathcal{V}) \subset \mathcal{L}_2(\mathfrak{C})$. \square

It is important to note that the \mathcal{L}_i -consistency defined in Def.3 is a weakened notion of consistency across causal models since any model might only agree on a single distribution of a given level $p \in \mathcal{L}_i$. Due to the nature of iVGAE being a compact model class opposed to a neural copy of an SCM, this is the only consistency achievable. However, it is not a negative impossibility result, on the contrary, iVGAE can perform any causal inference within the first two rungs of the PCH when provided with the corresponding data and sufficient model capacity i.e., the trade-off in expressivity solely comes from the fact that a compression on the model description is being performed. An important corollary to Thm.3 is that the CHT still applies across settings. That is, causal inferences within iVGAE as choice of parameterization remain sensible since the layer boundaries are strict.

Corollary 2. (iVGAE Partial Causal Hierarchy Theorem.) Consider the sets of all SCM and iVGAE, Ω, Υ , respectively. If for all $\mathcal{V} \in \Upsilon$ it holds that \mathcal{V} is $\mathcal{L}_1^p(\mathcal{V}) = \mathcal{L}_1^p(\mathfrak{C}) \implies \mathcal{L}_2^q(\mathcal{V}) = \mathcal{L}_2^q(\mathfrak{C})$ with $\mathfrak{C} \in \Omega$, where $\mathcal{L}_i^p \subset \mathcal{L}_i$ is a selection p, q over the set of all level 1,2 distributions respectively, then we say that layer 2 of iVGAE collapses relative to \mathfrak{C} . On the Lebesgue measure over SCMs, the subset in which layer 2 of iVGAE collapses to layer 1 has measure zero.

Proof. The proof is analogue to (Xia et al. 2021; Bareinboim et al. 2020) and assumes Fact 1 (or Thm.1 for the latter) to define an SCM-collapse relative to some SCM \mathfrak{C}' . If layer 2 SCM-collapses to layer 1 relative to \mathfrak{C}' then any SCM \mathfrak{C} will follow the properties $\mathcal{L}_1^p(\mathfrak{C}) = \mathcal{L}_1^p(\mathfrak{C}')$ and $\mathcal{L}_2^k(\mathfrak{C}) = \mathcal{L}_2^k(\mathfrak{C}')$ for some set selections p, k . By Thm.3 we know that there will always exist a corresponding iVGAE \mathcal{V} that is \mathcal{L}_2 -consistent with \mathfrak{C} but since it is consistent with \mathfrak{C} and not \mathfrak{C}' it follows the equivalent properties $\mathcal{L}_1^p(\mathcal{V}) = \mathcal{L}_1^p(\mathfrak{C}')$ and $\mathcal{L}_2^k(\mathcal{V}) = \mathcal{L}_2^k(\mathfrak{C}')$, which means that the layer 2 also collapses for the iVGAE model. The analogue argument holds in reverse when layer 2 does not SCM-collapse to layer 1 relative to \mathfrak{C}' . Since both directions together suggest an equivalence on the way collapse occurs for both SCM and iVGAE, Fact 1 from (Xia et al. 2021) (or Thm.1 from (Bareinboim et al. 2020)) holds. \square

The iVGAE model is capable of causal inference but it cannot act as a complete reparameterization of an SCM since it lacks the same amount of model description, that is, an SCM models structural equations for each of the variables while iVGAE expresses a causal probabilistic model parameterized by two functions. A consequence of Thm.3 is thus that the general layer of counterfactuals (\mathcal{L}_3) cannot be inferred using the description in Def.5. While it is easy to see why this is the case, since iVGAE deploys a single model, it is important to consider Def.2 from (Bareinboim et al. 2020) to proceed with the proof.

Definition 7. (\mathcal{L}_3 Valuations.) Let \mathfrak{C} be an SCM, then for instantiations \mathbf{x}, \mathbf{y} of the node sets $\mathbf{X}, \mathbf{Y}, \mathbf{Z}, \mathbf{W} \dots \subseteq \mathbf{V}$

where $\mathbf{Y}_x : \mathbf{U} \mapsto \mathbf{Y}$ denotes the value of \mathbf{Y} under intervention \mathbf{x} , a counterfactual distribution is given by

$$p^{\mathcal{C}}(\mathbf{y}_x, \mathbf{z}_w, \dots) = \sum_{u \in \mathcal{U}} p(\mathbf{u}) \quad (20)$$

with $\mathcal{U} = \{\mathbf{u} \mid \mathbf{Y}_x(\mathbf{u}) = \mathbf{y}, \mathbf{Z}_w(\mathbf{u}) = \mathbf{z}, \dots\}$ being all noise instantiations consistent with $\mathbf{Y}_x, \mathbf{Z}_w, \dots$ representing different "worlds".

With Def.7 the simplicity of the proof for Cor.3 becomes evident, since a single iVGAE is not capable of representing the different (counter-factual) "worlds" implied by the different interventions $p(\mathbf{V}_i | do(\mathbf{V}_j)) = \mathbf{V}_{i, \mathbf{v}_j}$.

Corollary 3. (iVGAE Limitation.) For any SCM \mathcal{C} there exists no iVGAE \mathcal{V} such that \mathcal{V} is \mathcal{L}_3 -consistent w.r.t. \mathcal{C} .

Proof. For an iVGAE model \mathcal{V} to be \mathcal{L}_3 -consistent with an SCM requires \mathcal{V} to have the capability of inducing distributions from that layer $p^{\mathcal{V}} = p \sim \mathcal{L}_3$. Def.7 suggests that a counterfactual involves the instantiations of multiple worlds for any SCM \mathcal{C} , $p(\mathbf{V}_i | do(\mathbf{V}_j))$ for different tuples (i, j) . While \mathcal{V} is capable of modelling each of the $\omega_{ij} = p(\mathbf{V}_i | do(\mathbf{V}_j))$ jointly, it is not capable of accumulating the probability masses $p(\mathbf{u})$ for which \mathbf{u} is consistent with $\cup \omega_{ij}$ since it is a single model that directly estimates the l.h.s. of Eq.8 opposed to an algorithmic procedure of checking over all possible instances \mathbf{u} for consistency. \square

Proof for Corollary 4

While Thm.3 points out that iVGAE are causally expressive and that their existence is theoretically guaranteed, the following corollary is an important consequence that reduces the search space for such an iVGAE in practice significantly. That is, the induced graph \mathcal{G} of any SCM \mathcal{C} can be inducted into the GNN layers of the iVGAE such that \mathcal{L}_2 -consistency is still warranted.

Corollary 4. (\mathcal{L}_2 Representation.) For any SCM \mathcal{C} that induces a graph \mathcal{G} , there exists a corresponding iVGAE $\mathcal{V} = (q, p)$ where q, p are \mathcal{G} -GNN layers such that \mathcal{V} is \mathcal{L}_2 -consistent with \mathcal{C} .

Proof. We repeat the arguments of the proof in Thm.3 with the slight modification that $\mathcal{V} := \mathcal{V}^{\mathcal{G}}$, indicating the \mathcal{G} -GNN layers p, q , where \mathcal{G} is the SCM \mathcal{C} induced graph. \square

Proof for Theorem 4

While expressivity is an important property of any model for inferential processes in science, identifiability stands at the core of causal inference. That is, using partial information on higher levels of the PCH (or of the SCM) to perform inferences starting from the lower levels. E.g., inferring the causal effect of X on Y denoted by $p(Y | do(X))$ using only observational data from $p(X, Y)$ requires the identification of an estimand in the purely causal setting. If the graph is given by $X \rightarrow Y$, then the identification is given by the conditional $p(Y | X) = p(Y | do(X))$. However, if the structure is more involved, imagine a (hidden) confounder Z such that $X \leftarrow Z \rightarrow Y$, then an adjustment regarding

Z 's influence would be interesting. Pearl's *do*-calculus provides an graphical-algebraic tool for performing identification (Pearl 2009). Thm.4 establishes that these causal inferences are equivalent between the domains. In a nutshell, if one can perform an identification of inference for an SCM, one can also do it for an iVGAE model.

Theorem 4. (Dual Identification.) Consider the causal quantity of interest $Q = p^{\mathcal{C}}(\mathbf{V}_i | do(\mathbf{V}_j))$, \mathcal{G} the true causal graph underlying SCM $\mathcal{C} \in \Omega$ and $p(\mathbf{V})$ the observational distribution. Q is neurally identifiable from iVGAE $\mathcal{V} \in \Upsilon$ with \mathcal{G} -GNN modules iff Q is identifiable from \mathcal{G} and $p(\mathbf{V})$.

Proof. The proof uses the same trick as the proof for Thm.4 in (Xia et al. 2021) to establish the duality in identification for SCM and iVGAE. Let Ω, Υ be the sets of all SCMs and iVGAEs respectively. If Q is not identifiable from a graph \mathcal{G} and the observational distribution $p(\mathbf{V})$ with full support $\forall \mathbf{v} : p(\mathbf{v}) > 0$, then there exists a pair of SCMs $\mathcal{C}, \mathcal{C}'$ such that they agree on \mathcal{L}_1 and \mathcal{G} but not on \mathcal{L}_2 i.e., $p^{\mathcal{C}}(\mathbf{V}_i | do(\mathbf{V}_j)) \neq p^{\mathcal{C}'}(\mathbf{V}_i | do(\mathbf{V}_j))$. By Cor.4 we know that there will always be an iVGAE model $\mathcal{V}^{\mathcal{G}}$ based on \mathcal{G} -GNN layers that is \mathcal{L}_2 -consistent with \mathcal{C} . This is all, since, $p^{\mathcal{V}^{\mathcal{G}}}(\mathbf{V}_i | do(\mathbf{V}_j)) = p^{\mathcal{C}}(\mathbf{V}_i | do(\mathbf{V}_j)) \neq p^{\mathcal{C}'}(\mathbf{V}_i | do(\mathbf{V}_j))$ which suggests that if Q is not identifiable by \mathcal{G} and $p(\mathbf{V})$, then it is also not neurally identifiable through $\mathcal{V}^{\mathcal{G}}$. Again, as in the proof for Cor.2, the reverse direction where Q is assumed to be identifiable holds true for the same reason. \square

Further Experimental Insights and Details

The following subsections provide an extensive empirical analysis of causal effect estimation (I), the identification thereof (II) and properties of the density estimation (III). We make our code publically available at <https://anonymous.4open.science/r/Relating-Graph-Neural-Networks-to-Structural-Causal-Models-A8EE>.

Causal Effect Estimation/Identification

Our experiments in the following investigate two important aspects from causal inference, namely causal effect estimation (I) and identification (II). In (I) we are interested in the average causal/treatment effect (Eq.12, (Pearl 2009; Peters, Janzing, and Schölkopf 2017)), defined as $ATE(X, Y) := \mathbb{E}[Y | do(X=1)] - \mathbb{E}[Y | do(X=0)]$, where the binary variable X is being referred to as treatment. Note that we can extend the ATE to be categorical/continuous, however, we focus on binary structures in the following, thereby the mentioned formulation is sufficient. Also, note that ATE is a special case of density estimation in which the same intervention location X is being queried for the different intervention parameterizations $do(X = x)$, for binary variables this amounts to $do(X = i), i \in \{0, 1\}$. General properties of the density estimation for the iVGAE are being systematically investigated in later sections of the Appendix (Figs.7,8). For (II) we are going to deviate slightly from the regular notion of identification. In identification, one is interested in obtaining the causal quantity of interest $p(Y | do(X))$ in terms of purely observational data $p(X, Y)$. Generally, this is impossible as the CHT suggests (Bareinboim et al. 2020), how-

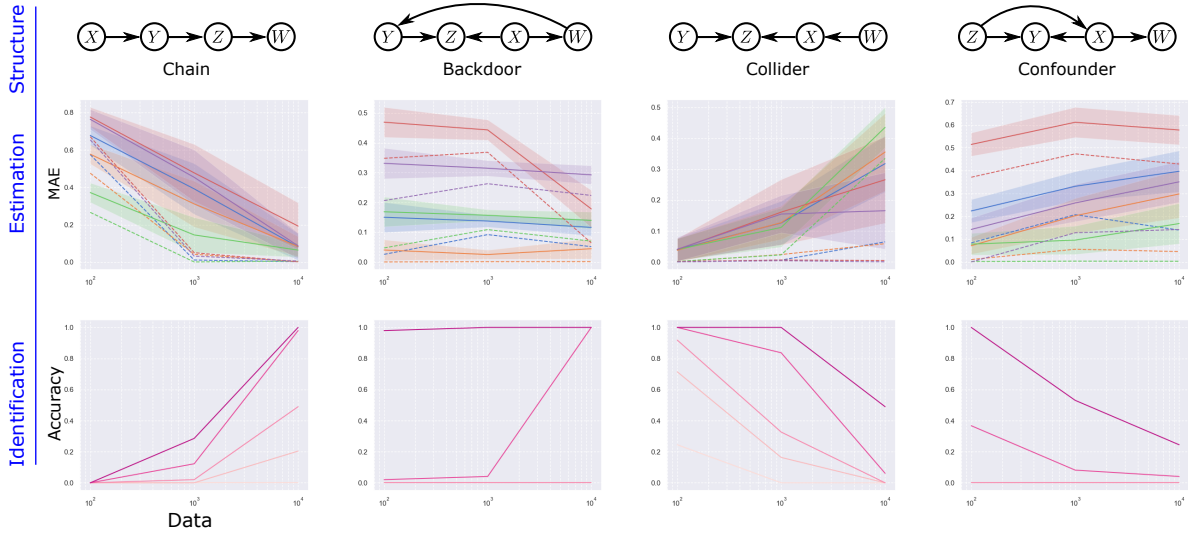


Figure 6: **Causal Effect Estimation and Identification.** Elaboration alongside details are to be found in the corresponding text segment of the Appendix. Four different structure families are being presented (top row). Each of the structures is being generated according to the base definition and randomly parameterized 5 times. For each of these parameterizations 7 random seeds of iVGAE models are being trained and each same-colored mean and best performance lines are being plotted on a log-datasize scale (middle row). The identification accuracy of the structure, independent of parameterizations, is being plotted using the thresholds tests, a darker color refers to a tolerance increase (bottom row). (Best viewed in color.)

ever, using partial causal knowledge (e.g. on the underlying graph structure) one can in fact identify any causally sufficient Markovian SCM i.e., SCMs with no hidden confounding or dependent exogenous terms (Pearl 2009). For neural-causal models, NCMs, this was shown in (Xia et al. 2021). Since the iVGAE is a data-dependent model (Def.4,Thm.4) it can not act as a proper SCM like NCM can. The iVGAE trades complexity for expressivity, thereby classical identification is not possible and thus in the following refer to identification as the capability of *generally identifying a given structure independent of its parameterization*. For this, we can deploy a threshold based test similar to the test introduced for NCMs by (Xia et al. 2021) i.e., if the iVGAE \mathcal{V} can model the selected distributions of the family of SCMs $\mathfrak{F}_G = \{\mathfrak{C} \mid \mathfrak{C} \models G\}$ that all model the same structure G at the second-level of the PCH sufficiently well, mathematically $|\mathcal{L}_2^p(\mathcal{V}) - \mathcal{L}_2^p(\mathfrak{F})| < \tau$ for some subset p where $\tau \in \mathbb{R}$ is the threshold, then the structure has been identified. In the following, Fig.6 will act as guiding reference to the subsequent elaborations. We make our code publically available at <https://anonymous.4open.science/r/Relating-Graph-Neural-Networks-to-Structural-Causal-Models-A8EE>.

Considered SCM Structures. We consider four different structural causal models structures (1: chain, 2: backdoor, 3: collider, 4: confounder) that are of significantly different nature in terms of information flow as dictated by the d -separation criterion (Koller and Friedman 2009; Pearl 2009). Fig.6 portraits the different structure (note the re-ordering of the variables, the graphs are being drawn in a planar manner). In the following we provide the exact parametric form

for each of the SCMs $\mathfrak{C}_i, i \in \{1..4\}$, the chain is given by

$$\mathfrak{C}_1 = \begin{cases} X \leftarrow f_X(U_X) = U_X \\ Y \leftarrow f_Y(X, U_Y) = X \wedge U_Y \\ Z \leftarrow f_Z(Y, U_Z) = Y \wedge U_Z \\ W \leftarrow f_W(Z, U_W) = Z \wedge U_W, \end{cases} \quad (21)$$

the backdoor structure is given by

$$\mathfrak{C}_2 = \begin{cases} X \leftarrow f_X(U_X) = U_X \\ Y \leftarrow f_Y(W, U_Y) = W \oplus U_Y \\ Z \leftarrow f_Z(X, Y, U_Z) = X \vee (Y \wedge U_Z) \\ W \leftarrow f_W(X, U_W) = X \vee U_W, \end{cases} \quad (22)$$

the collider is given by

$$\mathfrak{C}_3 = \begin{cases} X \leftarrow f_X(W, U_X) = W \wedge U_X \\ Y \leftarrow f_Y(U_Y) = U_Y \\ Z \leftarrow f_Z(X, Y, U_Z) = X \vee (Y \wedge U_Z) \\ W \leftarrow f_W(U_W) = U_W \end{cases} \quad (23)$$

and finally the confounded structure is

$$\mathfrak{C}_4 = \begin{cases} X \leftarrow f_X(Z, U_X) = Z \vee U_X \\ Y \leftarrow f_Y(X, Z, U_Y) = (X \wedge U_Y) \oplus (Z \wedge U_Y) \\ Z \leftarrow f_Z(U_Z) = U_Z \\ W \leftarrow f_W(X, U_W) = X \wedge U_W, \end{cases} \quad (24)$$

where \oplus denotes the logical xor-operation. We refer to logical operations to assert that the variables remain within $\{0, 1\}$. Note that we consider Markovian SCM, thus the exogenous/noise terms are independent. We choose Bernoulli

$\mathcal{B}(p), p \in [0, 1]$ distributions for the noise terms. We choose the p_i for each of the terms U_i uniformly at random to generate 5 different parameterizations of the same structure. For each intervention we create a data set of size 10000 and train a model consisting of two iVGAE modules. We consider 7 random seeds for each of the 5 parameterizations for each of the 4 structures, $7*5*4=140$ distinct optimizations. In the following we always consider the ATE of X on Y , that is $Q = \text{ATE}(X, Y)$, which can be positive/negative $Q \neq 0$ or neutral $Q = 0$ if their is neither a direct nor indirect influence from X to Y . For the identification accuracy calculation we consider thresholds $\tau \in \{0.01, 0.05, 0.1, 0.2, 0.3\}$.

Interpretation for Estimation (I) and Identification (II) on the chain structure \mathfrak{C}_1 . Consider the first column in Fig.6. For (I) we clearly observe the mean performances of the different models to reduce the mean absolute error (MAE) with increased data amount. Note that intervention is akin to conditioning on this graph and that the causal effect is present and positive for any of the parameterizations. The dotted lines represent the best performances. Some optimizations start off more ideal but converge less fast. When inspecting closely, we observe that the error is non-zero for two reasons, one, that the we keep capacity consistent and don't perform parameter tuning, and second, that the Bernoulli-chain will oftentimes lead to low values for the tail of the chain W for which numerical stability becomes an issue. For (II) we can affirmatively conclude that for any of the thresholds the classification of the structure is successful and improves with the number of training steps. The lowest threshold depends on the base error, which we reason to be induced by W , which explains the zero-line.

Interpretation for Estimation (I) and Identification (II) on the backdoor structure \mathfrak{C}_2 . Consider the second column in Fig.6. For (I) we observe a more involved scenario in which there is a trend towards improvement through data increase but not amongst all parameterizations of this backdoor SCM. Here X has only an indirect effect on Y via the backdoor W . The ATE can be positive/negative/neutral depending on the parameterization. While generally the same message is being posed as for the chain, we argue that here we observe the influence of ELBO i.e., that the optimization is non-convex and we can only achieve local optimality. That is, the variance in the quality of fits for the trained models is significantly larger than for the chain. We believe this to be due to the increased complexity in structure. We have a backdoor from $X \rightarrow W \rightarrow Y$ but also a collider on Z , $Y \rightarrow Z \leftarrow X$. For (II) the relaxed threshold will be trivially true, since the average modelling error across parameterizations is better as with e.g. the chain structure. The threshold $\tau = 0.2$ suggest informativeness over data, as intended, while the other thresholds collapse to the zero-line as previously for the chain.

Interpretation for Estimation (I) and Identification (II) on the collider and confounded structures $\mathfrak{C}_3, \mathfrak{C}_4$. Consider the two rightmost columns in Fig.6. We cover both structures at once, since both the results for (I) and (II) are indicative of the same underlying behavior, just at different

scales for the considered settings. For the collider we note that there exists only the neutral ATE while for the confounder, like for the backdoor, any ATE value is feasible. For (I) in both structures we generally observe a trend towards error increase with increasing model optimization independent of parameterizations. While this might appear as a grave failure of the trained models, a closer inspection reveals that the uniform random initial state for \mathfrak{C}_3 is the gold standard since the ATE is zero. Some of the dotted lines (e.g. purple or red) in fact stay at that level. In a nutshell, the model can only remain at an optimum or become worse since any change in the target distribution will increase the error. In the confounder \mathfrak{C}_3 we observe similar phenomena. The identification results (II) mirror these observations.

Numerical Report. In Tab.1 we show numerical statistics on the trained models applied to the different SCM structures \mathfrak{C}_i for one of the 5 parameterizations averaged across 7 random seeds. We show the two interventions on X for computing the ATE, and report mean, best and worst ELBO (Def.2) and likelihood $\log p(x)$ performances (the higher the better). As expected, ELBO lower bounds the marginal log-likelihood and the validation performance, as desired, corresponds with the test performance.

Systematic Investigation on Density Estimation

We perform multiple experiments to answer various interesting questions. The following list enumerates all the key **questions** to be highlighted and discussed in this section:

- (a) What aspects of an interventional change through $do(\cdot)$ does the method capture?
- (b) How does variance in ELBO 2 during variational optimization affect the method?
- (c) When and how does the method fail to capture interventional distributions?
- (d) At what degree does the performance of the method vary for different training durations?
- (e) How does the method's scaling towards many interventions behave when keeping capacity constant?
- (f) How important is parameter tuning?

For all the subsequent experiments we considered the same architecture. That is, an iVGAE (Def.5) model consisting of two interventional GNNs (Def.1) for the encoder and decoder respectively where each GNN consists of 2 Sum-Pool Layers as introduced by (Kipf and Welling 2016a). The decoder has $2B^2$ parameters, whereas the encoder has $3B^2$ parameters, where B is the batch size, to allow for modelling the variance of the latent distribution. We consider datasets of size 10000 per intervention. The interventions are collected by modifying the data generating process of the data sets. For simplicity, we mostly consider uniform interventions. Optimization is done with RMSProp (Hinton, Srivastava, and Swersky 2012) and the learning rate is set to 0.001 throughout. We perform a mean-field variational approximation using a Gaussian latent distribution and a Bernoulli distribution on the output. All data sets we have considered are binary but extensions to categorical or continuous domains follow naturally. In the following, we focus

on ASIA introduced in (Lauritzen and Spiegelhalter 1988), and Earthquake/Cancer covered within (Korb and Nicholson 2010) respectively. We employ a training, validation and test set and use the validation set to optimize performance subsequently evaluated on the test set. We use a 80/10/10 split. We use 50 samples per importance sampling procedure to account for reproducibility in the estimated probabilities. Training is performed in 6000 base steps where each step considers batches of size B that are being scaled multiplicatively with the number of interventional distributions to be learned. The adjacency provided to the GNNs is a directed acyclic graph (DAG) summed together with the identity matrix to allow for self-reference during the computation. The densities are acquired using an adjusted application of Alg.1. All subsequent experiments are being performed on a MacBook Pro (13-inch, 2020, Four Thunderbolt 3 ports) laptop running a 2,3 GHz Quad-Core Intel Core i7 CPU with a 16 GB 3733 MHz LPDDR4X RAM on time scales ranging from a few minutes up to approximately an hour with increasing size of the experiments. In the following, Figs.7 and 8 act as reference for the subsequent subsections' elaborations on the questions (a)-(f). Numerical statistics are provided in Tab.2. For reproducibility and when reporting aggregated values (e.g. mean/median) we consider 10 random seeds. Our code is available at <https://anonymous.4open.science/r/Relating-Graph-Neural-Networks-to-Structural-Causal-Models-A8EE>.

Q-(a) What aspects of an interventional change through $do(\cdot)$ does the method capture? Consider Fig.7(a) in the following. It shows an iVGA model trained on the observational (\mathcal{L}_1) and one interventional (\mathcal{L}_2 , intervention $do(tub = \mathcal{B}(\frac{1}{2}))$) distributions, where the former is shown on the left and the latter on the right. We can observe that both the change within the intervention location (tub) but also in the subsequent change propagations along the causal sequence (either, xray, dysp) are being captured. In fact, they are being not only detected but also adequately modelled for this specific instance. If the optimization is successful in fitting the available data with the available model capacity, then this is the general observation we make across all the other settings we have evaluated i.e., the model can pick-up on the interventional change without restrictions.

Q-(b) How does variance in ELBO 2 during variational optimization affect the method? Consider Fig.7(b) in the following. Two different random seeds (that is, different initializations and thus optimization trajectories) for the same iVGA under same settings (data, training time, etc.) are being shown. Clearly, the optimization for the seed illustrated on the left was successful in that the quantities of interest are being adequately estimated. However, the random seed shown on the right overestimates several variables (tub, either, xray) and simply does not fit as well. We argue that this is a general property of the variational method and ELBO (Eq.2) i.e., the optimization objective is non-convex and only a local optimum is guaranteed. Put differently, the variance in performance amongst random seeds (as measured by ELBO) is high.

Q-(c) When and how does the method fail to capture interventional distributions? Consider Fig.7(c) in the following. The predicted marginals of a single iVGA model on the Earthquake dataset (Korb and Nicholson 2010) are being presented for the observational density (right) and the interventional $do(Earthquake = \mathcal{B}(\frac{1}{2}))$ (left). The underlying graph in this real-world inspired data set is given by

$$G = (\{B, E, A, M, J\}, \{(B \rightarrow A), (E \rightarrow A), (A \rightarrow \{M, J\})\}) \quad (25)$$

where B, E, A, M, J are Burglary, Earthquake, Alarm, MaryCalls and JohnCalls respectively. From G we can deduce that the mutilated graph G_I that is generated by the aforementioned Bernoulli-intervention $I = do(E = \mathcal{B}(\frac{1}{2}))$ will in fact be identical $G = G_I$. Put differently, conditioning and intervening are identical in this setting. The formulation for performing interventions in GNN (Def.1) only provides structural information i.e., information about the intervention location (and thus occurrence) *but not about the content of the intervention*. While this generality is beneficial in terms of assumptions placed onto the model, it also restricts the model in this special case where associational and interventional distributions coincide. In a nutshell, computationally, the two posed queries $I_1 = I$ and $I_2 = do(\emptyset)$ are identical in this specific setting ($I_1 = I_2$) and this is also being confirmed by the empirical result in Fig.7(c) i.e., the predictions are the same across all settings as follows naturally from the formulation in Def.1 which in this case is a drawback. Generally, this insight needs to be considered a drawback of formulation Def.1 opposed to being a failure mode since the formulation indeed behaves as expected. In all our experiments, actual failure in capturing the densities seems to occur only in low model-capacity regimes, with early-stoppage or due to numerical instability.

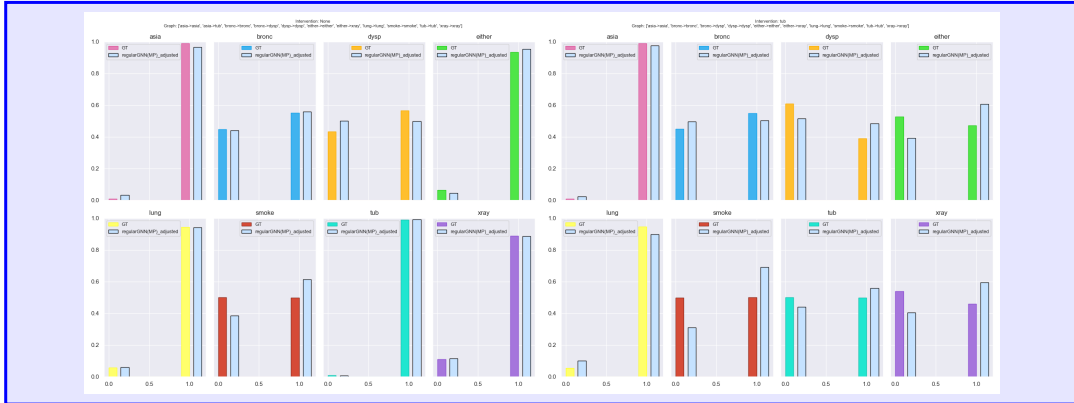
Q-(d) At what degree does the performance of the method vary for different training durations? Consider Fig.8(d) in the following. It shows the same model being probed for its predictions of the observational distributions at different time points, left early and right later (at convergence). Following intuition and expectation, training time does increase the performance of the model fit. Consider nodes tub and lung which were both underestimating in the earlier iterations while being perfectly fit upon convergence.

Q-(e) How does the method's scaling towards many interventions behave when keeping capacity constant? Consider Fig.8(e) in the following. We show the same iVGA model configurations being trained on either 2 interventional (top row) or 4 interventional distributions from the Earthquake dataset (Korb and Nicholson 2010). I.e., we keep the model capacity and the experimental settings consistent while increasing the difficulty of the learning/optimization problem by providing double the amount of distributions. As expected, we clearly see a degeneration in the quality of density estimation. The iVGA model trained on 2 distributions adequately estimates the Bernoulli-interventional distribution $do(A = \mathcal{B}(\frac{1}{2}))$ (top right) while the model trained on more distributions (lower right) fails.

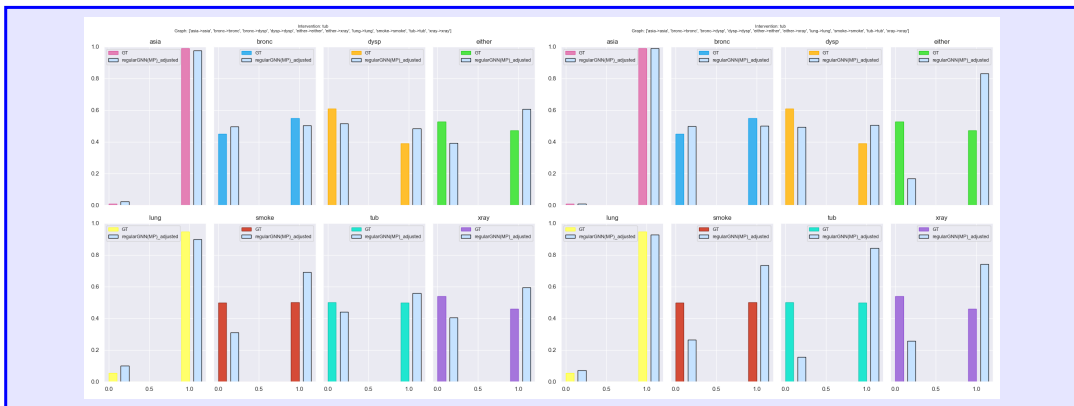
Q-(f) How important is parameter tuning? Consider Fig.8(f) in the following. It shows an iVGAE model before (left) and (after) parameter tuning on the Bernoulli-intervention $do(tub = \mathcal{B}(\frac{1}{2}))$ on the ASIA dataset (Lauritzen and Spiegelhalter 1988) where the tuned parameters involve aspects like pooling (sum, mean), layer numbers, learning rate, batch size etc. We clearly see a an improvement towards a perfect fit for certain nodes (smoke, tub, either). As expected, parameter tuning, as for any other machine learning model, is essential for improving the predictive performance. Especially, for universal density approximation, as discussed in Thm.2, this is crucial - since in principle any density can be approximated with sufficient capacity and thus the dependence relies on the model itself but also on the optimization for optimality in practice.

Numerical Report. In Tab.2 we show numerical statistics on the trained models applied to the different data sets for answering the investigated questions (a)-(f). For reproducibility and stability, we performed 10 random seed variants per run. NaN values might occur for a single seed due to numerical instability in training, thus invalidating the whole run. We show the performance on different, increasing interventional data sets at various training iterations. We report mean, best and worst ELBO (Def.2) and likelihood $\log p(x)$ performances (the higher the better). Question (b) regarding the variance of ELBO becomes evident when considering the best-worst gaps. As expected, ELBO lower bounds the marginal log-likelihood. Also, by providing more distributions to learn, thus increasing difficulty, the quality of the fits in terms of ELBO/likelihood degenerates which is inline with what we observed regarding question (e). Finally, we might also note that the validation performance, as desired, corresponds with the test performance.

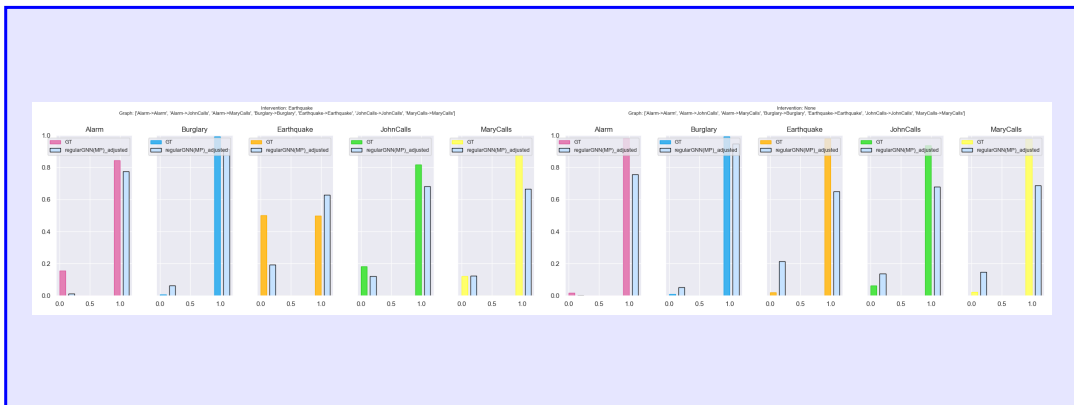
Full-width Figures and Tables. Following this page are the figures and tables (Fig.7, 8, Tabs.1, 2) that were referenced in the corresponding sections of the appendix.



(a)

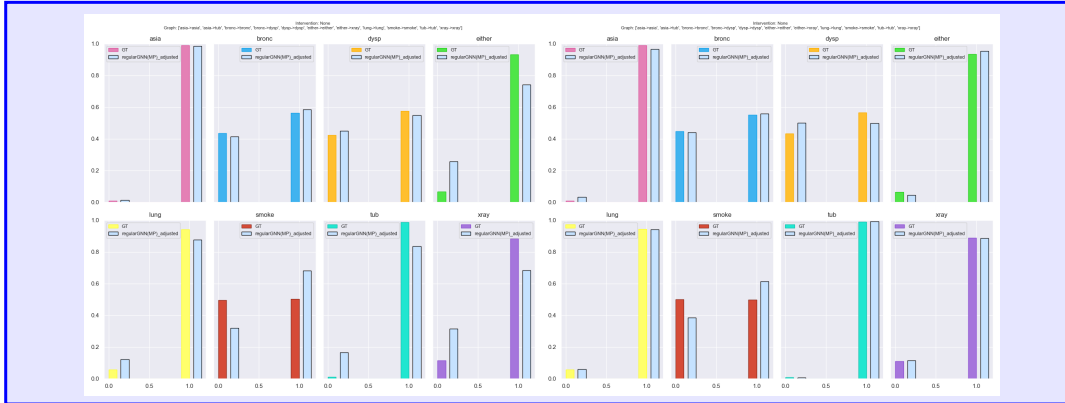


(b)

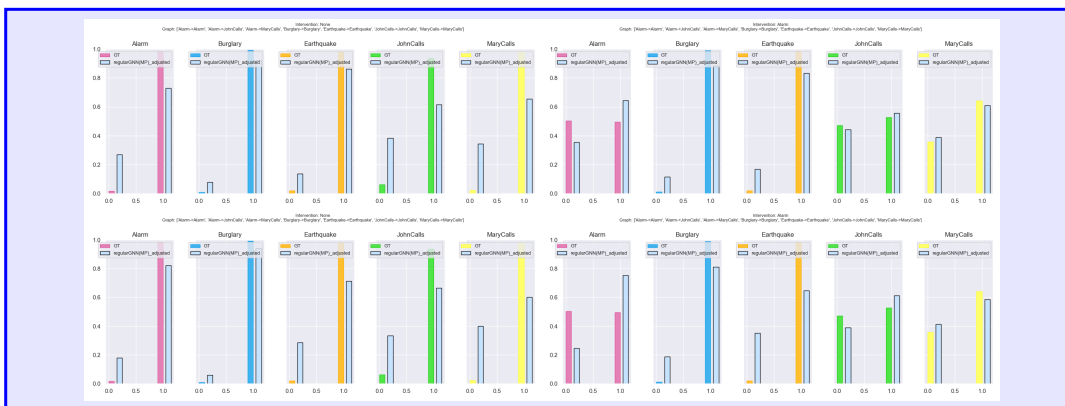


(c)

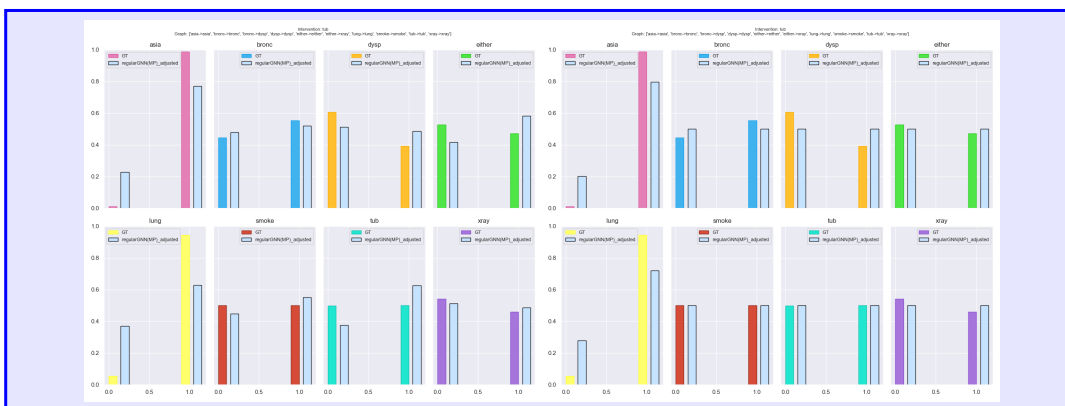
Figure 7: **Systematic Investigation: Questions (a), (b), and (c).** The questions being answered by the presented illustrations in the respective blue box are (a) What aspects of an interventional change through $do(\cdot)$ does the method capture? (b) How does variance in ELBO 2 during variational optimization affect the method? and (c) When and how does the method fail to capture interventional distributions? Please consider the elaboration within the corresponding text segment. (Best viewed in color.)



(d)



(e)



(f)

Figure 8: **Systematic Investigation: Questions (d), (e), and (f).** The questions being answered by the presented illustrations in the respective blue box are (d) At what degree does the performance of the method vary for different training durations? (e) How does the method's scaling towards many interventions behave when keeping capacity constant? and (f) How important is parameter tuning? Please consider the elaboration within the corresponding text segment. (Best viewed in color.)

\mathfrak{C}_i	$do(X = x)$	Steps	Mean Train ELBO	Mean Valid ELBO	Mean Test ELBO	Mean Valid $\log p(x)$	Mean Test $\log p(x)$	Best Test ELBO	Worst Test ELBO
1	1	2.5k	-1.48	-1.60	-1.59	-1.43	-1.43	-1.50	-1.86
1	0	2.5k	-1.86	-2.12	-2.07	-1.85	-1.84	-1.70	-2.47
2	1	2.5k	-1.48	-1.60	-1.59	-1.43	-1.43	-1.37	-1.86
2	0	2.5k	-1.86	-2.12	-2.07	-1.85	-1.84	-1.91	-2.47
3	1	2.5k	-1.48	-1.60	-1.59	-1.43	-1.43	-1.50	-1.86
3	0	2.5k	-1.86	-2.12	-2.07	-1.85	-1.84	-1.91	-2.47
4	1	2.5k	-1.48	-1.60	-1.59	-1.43	-1.43	-1.37	-1.86
4	0	2.5k	-1.86	-2.12	-2.07	-1.85	-1.84	-1.91	-2.47

Table 1: **Effect Estimation and Identification: Key Statistics.** The aggregations cover 7 random seeds per model.

Dataset	$ \mathcal{L}_2 $	Steps	Mean Train ELBO	Mean Valid ELBO	Mean Test ELBO	Mean Valid $\log p(x)$	Mean Test $\log p(x)$	Best Test ELBO	Worst Test ELBO
ASIA	2	16k	-3.43	-6.02	-4.60	-4.15	-4.11	-4.10	-5.37
ASIA	4	16k	NaN	NaN	-4.61	NaN	-4.05	-3.79	-5.59
Cancer	2	12k	-2.26	-4.76	-3.17	-3.66	-2.76	-2.35	-4.49
Cancer	4	12k	NaN	NaN	-3.26	NaN	-2.88	-2.43	-4.53
Earthquake	2	12k	-1.21	-3.02	-2.43	-1.92	-1.93	-1.49	-3.50
Earthquake	4	12k	-0.78	-4.67	-2.77	-2.31	-2.27	-1.75	-3.46

Table 2: **Density Estimation: Key Statistics.** The aggregations cover 10 random seeds for each of the models respectively.